Model for Pharmaceutical aerosol transport through stenosis airway

Puchanee Larpruenrudee[1], Mohammad S. Islam [1*], Gunther Paul[2], Akshoy R. Paul[3] Y.T. Gu[4] and Suvash C. Saha[1*]

[1]School of Mechanical and Mechatronic Engineering, University of Technology Sydney (UTS), 15 Broadway, Ultimo, NSW-2007, Australia

[2]James Cook University, Australian Institute of Tropical Health and Medicine, Townsville, QLD 4810, Australia

[3]Department of Applied Mechanics, Motilal Nehru National Institute of Technology Allahabad, Prayagraj 211004, Uttar Pradesh, India

[4]School of Mechanical, Medical and Process Engineering, Science and Engineering Faculty, Queensland University of Technology, Brisbane-4000, Australia.

Corresponding authors: **Suvash C. Saha,** Suvash.saha@uts.edu.au,
Mohammad S. Islam, mohammadsaidul.islam@uts.edu.au.

Chapter Abstract

Air pollution is the leading cause of different respiratory diseases such as asthma and chronic obstructive pulmonary disease (COPD) that commonly affect the respiratory health. Computational Fluid Dynamics (CFD) has been used to predict the airflow pattern and particle transport within human lungs under the disease conditions like obstructive airways. Nevertheless, the combination of the obstructive airways, as well as the aging impact on these diseases under the various flow rates and particle diameters, have not considered in the previous studies. This chapter provides a clear understanding of airflow characteristics and particle transport through obstructions and smaller airways due to aging based on an asymmetric lung model generating from the trachea to the fourth generation. Eight different lung models were used for the numerical simulation. The ANSYS Fluent 19.2 was employed to solve the problems under the finite volume discretization technique. Appropriate grid refinement has been performed for all cases. The results indicate that airflow pattern always changes at the stenosis area. The velocity significantly increases at stenosis area for the first two generations and the smallest diameter size. The maximum pressure drop was located at stenosis area for the first generation of right-lung and the fourth generation for the smallest diameter case, whereas the highest pressure was found in the trachea for both conditions. Stenosis areas at first two generations significantly affect higher turbulence intensity while smaller diameters generate lower turbulent fluctuation. The deposition efficiency and deposition fraction were based on the airway volume, particle size, and flow rate. The results of this study enhance the knowledge of airflow characteristics and particle deposition within asymmetric human lungs with stenosis area and smaller diameters.

8.1 Introduction

Air pollution is one of the critical factors that have threatened human health for a long time. In the early twentieth century, people worldwide were aware of the health effects that were caused by air pollution. Especially in London in 1952, the “killer fog” was the cause of death over 12,000 people (Davis et al. 2002). According to the World Health Organization (2020), over 7 million deaths were caused by air pollution effects in terms of both ambient and household air pollutions. The effects of this pollution can cause many diseases, particularly in respiratory diseases. In Australia, coal mining is one of the main air pollutants that directly affect respiratory disease, comparing to other works (Hendryx et al. 2020).

Although the respiratory system has many defense mechanisms to protect internal organs from foreign substances, air pollutants can still pass through those mechanisms. By the main factors, that cause the penetrative processes, are the size and chemical nature of the air pollutants (D’Amato et al., 2010). Several recent articles (Guan et al. 2016; Schiavoni, D’Amato & Afferni 2017; Hu, Zhong & Ran 2015; Kurt, Zhang & Pinkerton 2016; Yao & Rahman 2011; Kim et al. 2018) have examined the effect of air pollution to the risk of respiratory diseases such as asthma, respiratory infections and chronic obstructive pulmonary disease (COPD). They point out that this pollution can increase the risk of respiratory diseases for both adults and children. Chronic asthma and COPD are two of the respiratory diseases that have significantly affected human health worldwide since 1990. Based on the reports from the Australian Institute of Health and Welfare 2019, the majority of deaths were caused by COPD. From the statistics of deaths in 2017, over 7,500 deaths were caused by COPD from among aged over 55 years, whereas 400 deaths were led by asthma from among aged 5 years to 34 years. For worldwide deaths from diseases, both asthma and COPD are the leading cause of death and injury in clinical treatment (Vicente et al., 2010). The evidence from the clinical treatment of Ahmed & Athar (2015), report that the mortality and morbidity from these diseases often occur because of over having intrinsic positive end-expiratory pressure (PEEPi) and dynamic hyperinflation (DH). By this point, it can create overwork of breathing (WOB).

In some cases, mechanical ventilation is used for the patients who cannot breathe by themselves because of the problems from the exhaustion of respiratory muscles (Vicente et al., 2010; Ahmed & Athar 2015). Some recent articles (Dominici et al. 2006; Gauderman et al. 2004; Moss & Oldman 2006; Ma & Lutchen 2009) have studied the characteristics of airborne particulate matter with causes respiratory diseases. They have found that having accurate data on the estimation of aerosol deposition within the human respiratory system is significant to

investigate and treat the disease's symptoms. Furthermore, it is also essential to estimate drug delivery in the case of mechanical ventilation patients (Dhand 2008; Dhand 2017; Dugernier et al. 2017). However, there are some difficult situations in terms of the ways of using mechanical ventilation because of having different airway characteristics. Normally, the respiratory system can completely grow and develop within 18-20 years of age (Mauderly & Hahn 1982; Polgar & Weng 1979). In contrast, the ability of the respiratory system will decrease among the elderly population. In this case, the lung structure will be changed with aging, which generates the alveolar dead space in the lung airways (Sharma & Goodwin 2006). The thickness of tissue within the lung airways tends to be based on aging. The diameter of the lung airways for the elderly between 50 to 80 years of age has been found to be smaller than other ages approximately 7% of reduction (Lai-Fook & Hyatt 2000). In terms of other ages, the diameter of the lung airways will decrease around 1% per year with the 30 years of age and later (Lai-Fook & Hyatt 2000; Faria et al. 2009). With this smaller diameter condition, the lung will need more pressure in order to change the volume in the lung. Therefore, the patient will have more difficulty in breathing (Kim et al. 2017).

Computational Fluid Dynamics (CFD) has been immensely used in Biomedical Science and Engineering, preferentially in the pharmaceutical industries. The reasons, that make CFD being widely used in this field, are the simulation abilities which provides the predictability and optimization in terms of inhaled therapies. It is also used to simulate the drug delivery process, which includes particulate, aerosol and gaseous drug types by starting from the entire process through lung airways (Tu, Yeoh & Liu 2012).

Previous studies in the last two decades have analyzed the airflow and particle deposition based on symmetric and asymmetric lung bifurcations from both realistic and non-realistic models. Most realistic models have generated from CT scans, whereas non-realistic models have created and developed from Weibel's model. Balashazy & Hoffman (1995) have examined the deposition of aerosols in both symmetric and asymmetric bifurcations and have found that the aerosols are mostly deposited firmly at the wall of a bifurcation. Nowak et al. (2002), have simulated the airflow and aerosol deposition by comparing between non-realistically lung model from Weibel (1963) and realistically lung model from CT scan. For this simulation, the lung model from G0 to G3 has been considered under the steady-state conditions for inhalation and exhalation. They state that the deposition fractions at bifurcations are totally the same for both models. Lee & Lee (2002), have generated the lung model based on Weibel's 1963 model with first four generations to study the aerosol dispersion whereas Liu et al. (2003), have studied the airflow characteristic of the asymmetric lung airway at the G5

to G11 of Weibel's 1963 model. The results of their studies indicate that the airways which having the different sizes, cannot affect the human breathing because of having the same airflow rate for both medial braches and their mother branches. At the same year, Kleinstreuer & Zhang (2003), have analyzed the target of aerosol deposition of the drug delivery within the symmetrically bifurcating at G3 to G6 under different hemispherical tumor conditions based on Weibel's 1963 model. The results of this study showed that the airflow pattern is based on the tumor size and inlet flow rate, whereas the particle deposition is based on the tumor size and upstream flow.

In some cases, the nanoparticle deposition has been considered based on Weibel's lung model. It has been focused on the mouth to the trachea through G3 to G5 and specific lung regions with a magnetic method (Shi et al. 2004; Zhang & Kleinstreuer 2004; Ghosh, Islam & Saha 2020). The authors concluded that the deposition efficiency is influenced by the nanoparticle size and inlet Reynolds numbers. Nanoparticle usually deposits at the bifurcation and inside the wall around the bifurcation. Moreover, nanoparticle deposition has an insignificant effect on turbulent fluctuations of upper airways. Cebral & Summers (2004) have studied the airflow through stenosis areas by using the realistic lung models and only considering at upper airways. The results from this study indicate that the pressure would decrease, whereas the shear stress would increase in the stenosis area. van Ertbruggen et al. (2004), have evaluated the gas flow and particle deposition by using a realistic model that starts from the trachea to G7 (the segmental bronchi). The authors summarized that an increase of inspiratory flow causes an increase of particle inertia that leads to greater deposition percentage. The main factors of deposition percentage also depend on the length, angles, diameters of branches. The literature survey on aerosol deposition from Borgstrom et al. (2006), have reported that the deposition at the throat region is a significant factor for lung deposition. Gemci et al. (2007), have studied the airflow in a 17-generation from a realistic model. The results demonstrate that the airflow characteristics within asymmetric airways are depended on the branching conduits. Ma & Lutchen (2009), have simulated the aerosol deposition in the upper airways based on a realistic model of the healthy lung. The different particle sizes from 1 to 30 μm have been used for this simulation. The results have shown that the deposition efficiency could be affected by particle sizes rather than the flow rate. They also point out that the turbulent flow will be generated only from the upper airway. Therefore, the model without the upper airway could not provide a realistic airflow within the lung. In contrast, there are some studies that consider focusing on the model starting at trachea region. In terms of drug delivery for the treatment of respiratory diseases, drug delivery efficiency can

be improved by an increase the dosage of the drug that transports to the disease area (Hess et al. 2005; Vestbo et al. 2013). To improve this efficiency, the trachea region is an important area where it should be prioritized to be a first step for the drug injection (Tsua, Henry & Butler 2011; Zhang & Kleinstresuer 2001).

The articles in this last decade examined the airflow and deposition patterns of the aerosol particles under various conditions such as particle sizes, velocity, and the airway's characteristics (Islam et al. 2017c; Islam et al. 2018a; Gu et al. 2019; Islam et al. 2019b; Saha et al. 2019; Rahman et al. 2019; Rahman et al 2020). Over than that, some authors have analyzed airflow and particle deposition based on the combination between helium and oxygen as known as heliox (Islam et al. 2018b; Islam et al. 2020a; Saha & Islam 2021). Saber & Heydari (2012), have analyzed the flow patterns and deposition fraction of particles between 0.1 μm to 10 μm at the upper airways from trachea to the third generations based on the healthy lung airway from the lung model of Weibel (1963). They reported that the number of deposition fraction is significantly based on the Stokes and Reynolds numbers. Srivastav et al. (2013) found the significant impact of the cartilaginous rings on airflow and particle transport through human airways. Srivastav et al. (2014) on another study, investigated the effects of particle deposition in a glomous tumour obstructed diseased human airways. They concluded from both the studies that the magnitude and location of maximum wall shear stress is an indication of probable wall injury.

Sul et al. (2014), have used the CFD to study the airflow characteristics in normal and obstructive airways. They only consider the lower airways between G8 to G14 for both symmetric and asymmetric models. The results from this study provide the clear understanding of shear stresses that are independent on the respiratory rate, but the shear stresses are dependent on the distribution of the obstructive areas within the lung. Augusto et al. (2015), have studied the aerosols deposition under three respiratory conditions that are inhalation, exhalation and breath-holding. In this case, four generations (G3 to G6 of Weibel's model) and three bifurcations model with 5 μm of particle sizes are considered to investigate the particle transport. The result shows that the number of aerosols deposition on the wall is higher for the breath-holding. The articles from Islam et al. (2017a) and Islam et al. (2017b), have examined the particle transport and particle deposition in a large scale 17^{th} generation based on the realistic lung model. It has found that the majority of smaller particles could escape from the 17^{th} generation and seem to continue flowing to the 23^{rd} generation. Zhang et al. (2018), have analyzed the particle deposition in realistic lung airways form CT scan. This article used the specific lung model for the COPD patient to compare with the healthy lung model. For the

stenosis location of COPD models, the results from this study indicated that the deposition efficiency and deposition fraction are affected by the stenosis areas. The deposition efficiency will increase in the same region of stenosis location, whereas the deposition fraction from the upper and lower lobes will decrease as a result of stenosis at the main bronchus.

Islam et al. (2019a), have studied and evaluated the particle transport and deposition in the lung airways from tracheal to 3rd generation of human airways. They have used three different lung models to compare the particle characteristics between the realistic and non-realistic lung models. For the non-realistic models, the first model is based on a symmetric lung model from Weibel's model, while the second model is developed to become an asymmetric lung model. The results showed that the airflow rate distribution of the realistic model is higher than the non-realistic models. Larger particle sizes have an essential effect on the turbulence deposition. Farghadan et al. (2019), have analyzed the particle transport in human lung airways in order to predict the particle source and destination for both inhalation and exhalation. They used a realistic lung model with defining the trachea region to be an injection area for 1 μm diameter. The result of their simulations indicates that the number of particles at the airway wall has a greater number than other regions. Islam et al. (2020b), have reviewed the airflow characteristics and particle deposition from the respiratory anatomical development. The results have found that both turbulence dispersion and flow rates, which are lower than 25 L/min, could not have a significant effect on deposition patterns of nanoparticle. Singh et al. (2020), have studied the airflow and particle transport through stenosis airways by employing the realistic model from CT scan based on the healthy human lung. The models have been reconstructed and created the random stenosis areas from 1st generation to 3rd generation. They have compared the stenosis area with the different cases that are stenosis at the left and right side of the main lung. Two main variables that are particle sizes and initial velocity, have been applied to evaluate the airflow and particle patterns. The authors report the results that stenosis airway could generate a complex-velocity. The deposition efficiency could increase, which is influenced by the flow rate and particle size.

The study from Koullapis et al. (2016), has examined the effect of the inlet velocity profile, inhalation flowrate and electrostatic charge for the particle deposition in the respiratory tract. The realistic model, which involves the upper airways through the lower airways from 1st generation to the 7th generation has been considered in this study. The authors state that the initial velocities have a significant effect on the particle deposition for the large sizes at the tongue, whereas the small particle sizes are often diffusible in the same area. The case study of Lalas et al. (2017), has particular analyzed the airflow and inhaled particles through the

comparison between three different lung airways that start from oral to 5th generation. By three different cases involves the normal lung airway, the abnormal lung airway with narrows in random areas, and the asymmetric lung model with narrows areas at the right side. In this case, the particle diameters from 1 to 30 μm are considered with only one flowrate of inlet velocity that is 12.6 L/min. For the results, the authors point out that the particles are often deposited in the opposite lung side from the inflammation areas. In terms of deposition fraction, the number of particle deposition is based on the particle sizes and particle densities.

From the recent articles, most of them mainly focus on the realistic model with having stenosis area at different generations, while the non-realistic model with stenosis areas are minority considered. In cases of non-realistic model, these articles only consider at the non-realistically symmetric model. There are only minority articles that focus on asymmetric model. Based on the recent studies, that using the realistic model, from Lalas et al. (2017), although this case study is useful for the medication, it does not consider the narrow airway at the 1st generation and only consider at one inlet velocity that is appropriate enough to transport the particle sizes from 1 to 10 μm. In contrast, Koullapis et al. (2016), state that the initial velocities have an essential effect on the particle deposition for both larger and smaller sizes. In order to enhance the understanding of the respiratory tract, the objective of this study aims to analyze the airflow and mainly considering particle transport of asymmetric lung model with stenosis sections at different generations from 1st generation to4th generation. Moreover, two main variables, which are initial velocity and particle diameter, will be applied to evaluate the effect that influences the airflow and particle transport. In terms of the breathing condition, an inhaled breathing condition will be considered in this chapter.

In case of the effects of aging on human lung airways, Phalen & Oldham (2001) and Isaacs & Martonen (2005) have studied the particle deposition within the lung under the function of age as children toward young adult between the age of 2 to 18 based on the particle sizes as 0.1 μm to 10 μm. There are few studies that have investigated these effects by comparing the normal lung to the emphysematous lungs as known as the senile lung in order to analyze the flow characteristic and the shear stress (Verbeken et al. 1992; Xia et al. 2010). Kim et al. (2017), have studied the characteristic of some mechanical properties based on the comparison between 50 and 80 years of age cases. The maximum pressure drop and shear stress were found from 80 years' cases. The authors report that one of the key aspects that could influence the change of mechanic properties is having different lung diameters. However, these studies only focus on the analysis as a group of age and do not consider the effect of flow rates. Therefore, this chapter will focus on the understanding in terms of aging involving adult's lung

and elderly's lung conditions that affect the airflow patterns and particle transport. Two different lungs which have different diameter will be analyzed based on the comparison between the normal asymmetric lung and the lungs that having smaller diameters.

8.2 Numerical Method

The conservation of mass and momentum assumptions were used to solve the fluid flow and particle transport:

$$\frac{\partial \rho}{\partial t} + \nabla \cdot (\rho \vec{v}) = S_m \tag{8.1}$$

Where, S_m is the mass source, and

$$\frac{\partial}{\partial t}(\rho \vec{v}) + \nabla \cdot (\rho \vec{v}\vec{v}) = -\nabla \rho + \nabla \cdot \left(\mu \left[(\nabla \vec{v} + \nabla \vec{v}^T) - \frac{2}{3}\nabla \cdot \vec{v}\mathrm{I}\right]\right) + \rho \vec{g} + \vec{F} \tag{8.2}$$

Where ρ is fluid static pressure

$\rho\vec{g}$ is a body force of gravity

$\vec{F}$ is a body force of external force (particle − fluid interaction)

In terms of flow characteristic, turbulent flow, which based on $k - \varepsilon$ model, was considered in this study. For the calculation of turbulent kinetic energy:

$$\frac{\partial(\rho k)}{\partial t} + \frac{\partial(\rho k u_i)}{\partial x_i} = \frac{\partial}{\partial x_j}\left[\frac{\mu}{\sigma_k}\frac{\partial_k}{\partial x_j}\right] + 2\mu_t E_{ij} E_{ij} - \rho \tag{8.3}$$

And for dissipation rate of an inertial frame:

$$\frac{\partial(\rho \varepsilon)}{\partial t} + \frac{\partial(\rho \varepsilon u_i)}{\partial x_i} = \frac{\partial}{\partial x_j}\left[\frac{\mu_t}{\sigma_\varepsilon}\frac{\partial_\varepsilon}{\partial x_j}\right] + \varepsilon_{1\varepsilon}\frac{\varepsilon}{k} 2\mu_t E_{ij} E_{ij} - \varepsilon_{2\varepsilon}\rho\frac{\varepsilon^2}{k} \tag{8.4}$$

Where, u_i is the velocity component in the corresponding direction

E_{ij} is the component of the rate of deformation

u_t is eddy viscosity

Based on Singh et al. (2020), there are some constants that were collected during numerous iterations of appropriated data for the turbulent flows:

$C_\mu = 0.09,\ \sigma_k = 1.00,\ \sigma_u = 1.30, C_{1\varepsilon} = 1.44,\ C_{2\varepsilon} = 1.92$

There are two variables of fluid flow within the lung airway. The main component is air which has the density at $1.225\ kg/m^3$ and viscosity at $1.7893 \times 10^5\ kg/ms$. The secondary component is aerosol which has the density at $1100\ kg/m^3$ under the discrete phase model. In terms of the method, particles were injected through the inlet surface at trachea under the surface injection method. The particle transport was calculated by:

$$\vec{F}_{D,i} = \frac{1}{2} C_D \frac{\pi d_{\rho,i}^2}{4} \rho (\vec{v}_{\rho,i} - \vec{v}) \left|\vec{v}_{\rho,i} - \vec{v}\right| \tag{8.5}$$

Where, C_D *is drag coefficient*

d_p *is particle diameter*

$\vec{v}_p$ *is the particle velocity*

The second law of Newton is employed for a single-particle motion i:

$$m_{p,i}\frac{\partial \vec{v}_{p,i}}{\partial t} = \vec{F}_{D,i} + m_{p,i}\vec{g} \tag{8.6}$$

The various particle sizes which include 1 μm, 2.5 μm, 5 μm, and 10 μm were used to be an injection at three different flow rates that involve 7.5 lpm, 15 lpm, and 30 lpm. The boundary conditions in this report were taken as the inlet velocity at trachea and outlet outflow at the end of fourth generation. In terms of wall conditions, stationary walls and no slip walls were used, while the boundary of wall conditions were based on the discrete phase model and a heat flux thermal. Under the discrete phase model, the wall was set to be used as a trap by the particle will be trapped when clashes the wall. See the summarize of properties as following (Table 8.1, 8.2).

Table 8.1: Air properties

Main component: It is considered as continuous phase	
Density (kg/m^3)	1.225
Viscosity (kg/ms)	1.7893×10^5

Table 8.2: Aerosol properties

Secondary component: It is considered as discrete phrase	
Density (kg/m^3)	1100
Particle size (μm)	1, 2.5, 5, 10
Inlet flow rate (lpm)	7.5, 15, 30

8.3 Geometrical Development

To enhance the understanding of the airflow and particle patterns of asymmetrical lung model, this study considers two different cases of asymmetric lung airways. In this section, all of the 3D models were created based on the smooth surface condition by using SolidWorks 2019 These models have been reconstructed from an asymmetric lung model from Islam et al. (2019a) which was based on a symmetric lung model from Weibel's lung model. The normal asymmetric lung model will be the basis of other lungs that have different airway's conditions. The diameter of branches at the right side were smaller than the left side around 25%.

The first case is the asymmetric lung model with having aging effects that cause a

smaller diameter for the whole lung model. The diameter for this case was reduced by 10% and 20% from normal asymmetric lung model. Seeing more information as Table 8.3toTable 8.5.

Table 8.3: The dimension of human lung airways for normal asymmetric lung

Number of generations	Location	Diameter				Length (cm)	Number
		Left Lung (cm)	Total cross-sectional area (cm^2)	Right Lung (cm)	Total cross-sectional area (cm^2)		
0	Trachea	1.80cm		2.54 cm^2		12.0	1
1	Bronchi	1.22	1.17	0.92	0.66	4.8	2
2	Bronchi	0.83	0.54	0.62	0.30	1.9	4
3	Bronchi	0.56	0.24	0.42	0.14	0.8	8
4	Bronchioles	0.45	0.16	0.34	0.09	1.3	16

Table 8.4: The dimension of human lung airways for asymmetric lung case with aging effects: with the reduction of 10%

Number of generations	Location	Diameter				Length (cm)	Number
		Left Lung (cm)	Total cross-sectional area (cm^2)	Right Lung (cm)	Total cross-sectional area (cm^2)		
0	Trachea	1.62 cm		2.06 cm^2		12.0	1
1	Bronchi	1.09	0.93	0.83	0.54	4.8	2
2	Bronchi	0.75	0.44	0.56	0.25	1.9	4
3	Bronchi	0.50	0.19	0.38	0.11	0.8	8
4	Bronchioles	0.41	0.13	0.31	0.08	1.3	16

Table 8.5: The dimension of human lung airways for asymmetric lung case with aging effects: with the reduction of 20%

Number of generations	Location	Diameter				Length (cm)	Number
		Left Lung (cm)	Total cross-sectional area (cm^2)	Right Lung (cm)	Total cross-sectional area (cm^2)		
0	Trachea	1.44 cm		1.63 cm^2		12.0	1
1	Bronchi	0.98	0.75	0.74	0.43	4.8	2
2	Bronchi	0.66	0.34	0.49	0.19	1.9	4
3	Bronchi	0.45	0.16	0.34	0.09	0.8	8
4	Bronchioles	0.36	0.10	0.27	0.06	1.3	16

The second condition is asymmetric lung model with stenosis area. There were five different

cases that were generated with the stenosis region in the different generation. All of these models used the same dimension except at the obstructive areas. The diameter in this area was reduced by 50% from the normal diameter of the normal airways. Moreover, the narrow airways were located in the random positions which start from 1st generation to 4thgeneration. See more detail as following (Table 8.6):

Table 8.6: The dimension of human lung airways for asymmetric lung case with stenosis areas

Number of generations	Location	Diameter				Length (cm)	Number	Diameter of stenosis area (cm)
		Left Lung (cm)	Total cross-sectional area (cm^2)	Right Lung (cm)	Total cross-sectional area (cm^2)			
0	Trachea	1.80cm		2.54 cm^2		12.0	1	-
1	Bronchi	1.22	1.17	0.92	0.66	4.8	2	0.46
2	Bronchi	0.83	0.54	0.62	0.30	1.9	4	0.31
3	Bronchi	0.56	0.24	0.42	0.14	0.8	8	0.21
4	Bronchioles	0.45	0.16	0.34	0.09	1.3	16	0.17

Figure 8.1a represents asymmetric lung airways without stenosis area. Figure 8.1b represents the stenosis section on the right side of the 1st generation. Figure 8.1c and 8.1d indicate the stenosis regions at the left and right sides of 2nd generation while Figure 8.1e and Figure 8.1f show the stenosis areas at the right side of 3rd generation and 4th generation respectively.

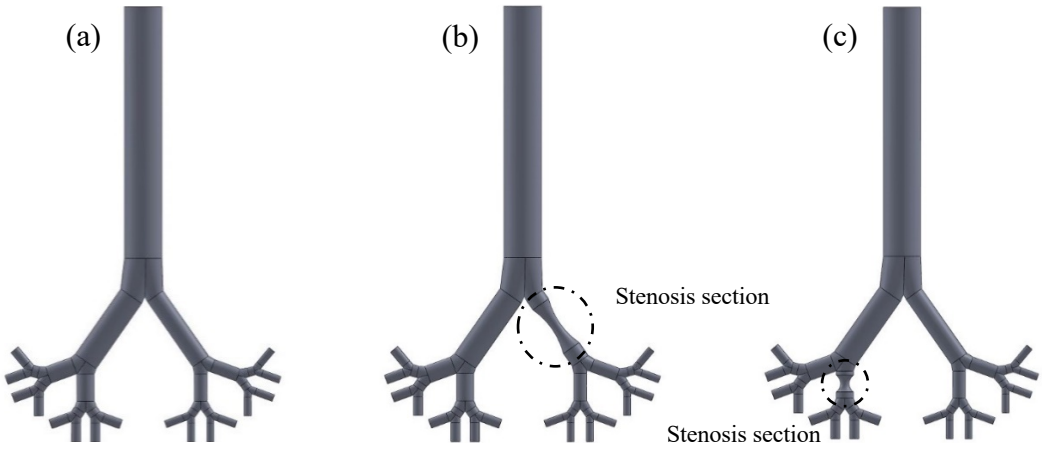

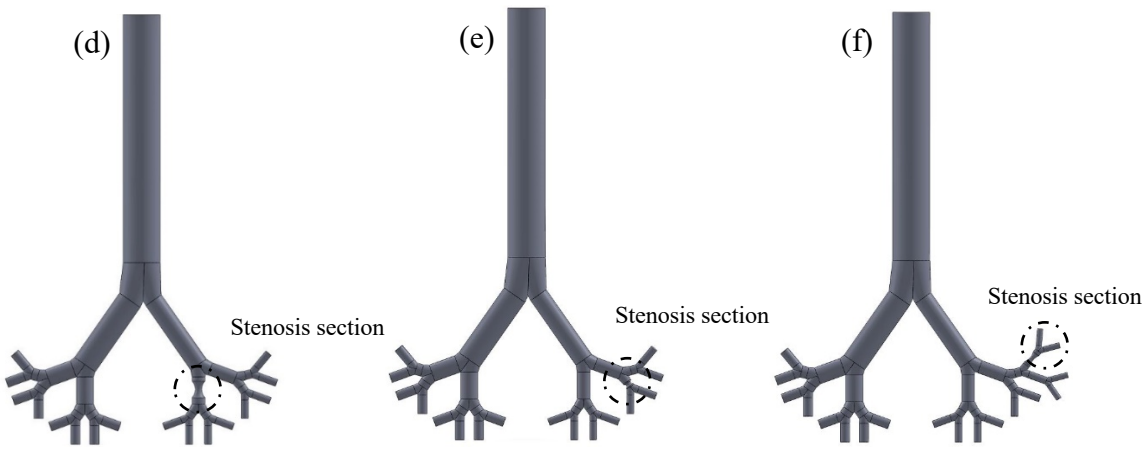

Figure 8.1 Reconstructed models of asymmetric lung airways: (a) normal asymmetric lung, (b) stenosis-right at 1st generation, (c) stenosis-left at 2nd generation, (d) stenosis-right at 2nd generation, (e) stenosis-right at 3rd generation, and (f) stenosis-right at 4th generation.

8.4 Grid Generation and Validation

Grid generation is an essential feature to bring the model to obtain the accurate result for CFD simulation. In order to get an appropriate grid refinement, considering at the mesh quality is the first aspect that should be prioritized. The ANSYS mesh module was used to generate the mesh for the whole geometry by using adapted sizing. However, there were some features that need to be used to control the flow characteristics inside the domain. Therefore, the inflation layer would be used to be a boundary to control the change of velocity and the particle movement inside the domain. In this study, the mesh generation for all of the models was generated based on the unstructured elements (Figure 8.2a). Figure 8.2b shows a boundary of inflation layer for the inside of the model. Figure 8.2c and 8.2d present the mesh at the entry trachea and outlet mesh of 3rd generation. Figure 8.2e and 8.2f represent the mesh at the stenosis area and mesh at a bifurcating branch, respectively.

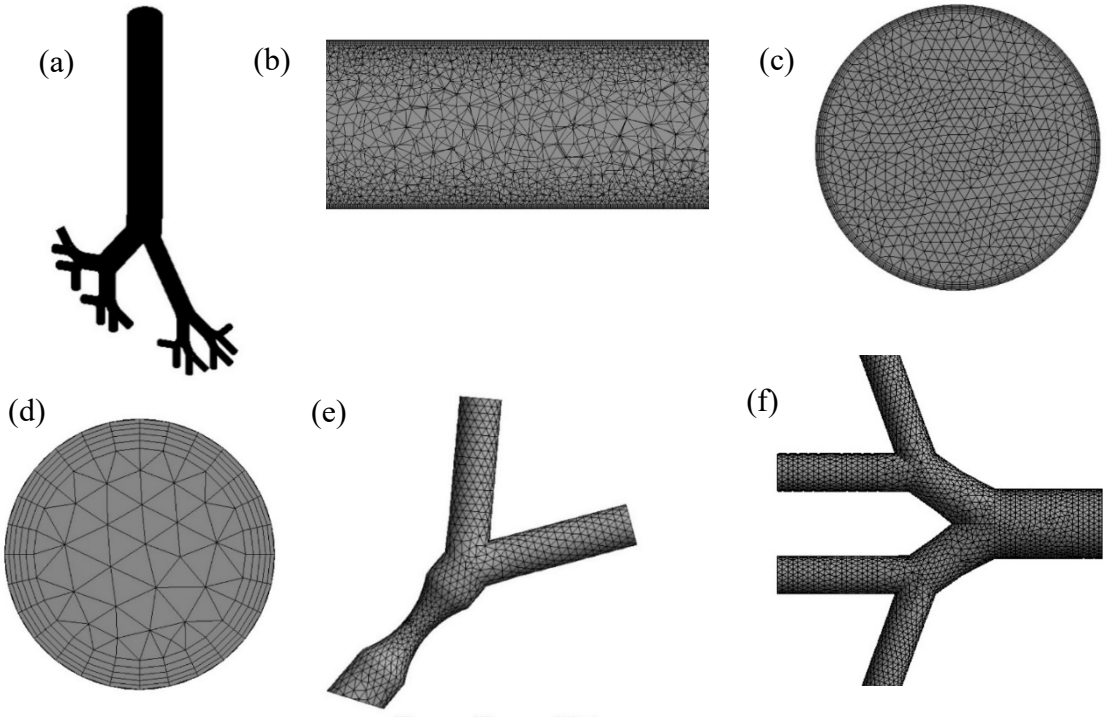

Figure 8.2 Unstructured mesh for the model: (a) the complete computational model, (b) inflation layer mesh near to the wall, (c) inlet mesh, (d) outlet mesh of 3rd generation, (e) mesh at stenosis area, and (f) mesh at a bifurcating branch

Grid refinement was generated based on flow condition and appropriate *y*+ value is selected as outlined in Sivastav et al. (2019). An orthogonal quality was applied to be the criteria to determine the mesh quality. The patch conforming method was also applied for the whole geometry. The model with the different number of elements was recalculated several times to obtain the maximum velocity for each time. After recalculation, the maximum velocities became stable when the number of elements could reach around 1.4 million (Figure 8.3a) with an average of minimum orthogonal quality around 0.13. Figure 8.3 presents the result for grid-independence test.

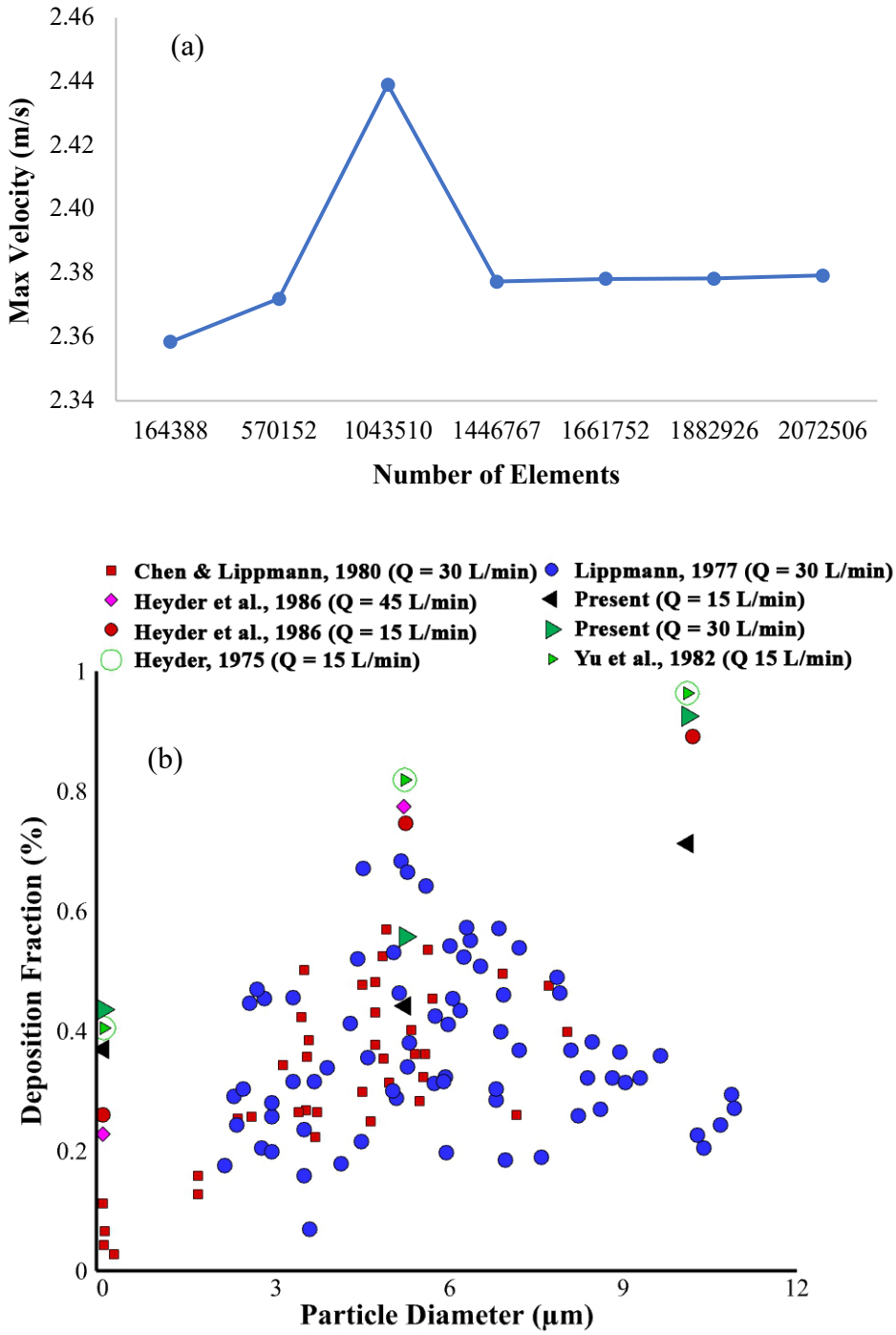

Figure 8.3 (a) Grid-independent for the maximum velocity: under the inlet condition at 30 lpm and (b) Deposition fraction comparison with published literatures (Chan & Lippmann 1980; Heyder et al. 1986; Lippmann 1977; Yu & Diu 1982).

The numerical results were compared with the available benchmark experimental and computational measurements (Chan & Lippmann 1980; Heyder et al. 1986; Lippmann 1977; Yu & Diu 1982). A mouth-throat model was used for the validation purpose as no similar stenosis model was found in the literature. Figure 8.3b showed the deposition fraction comparison at mouth-throat section for different flow rates. The numerical results were in the range of the experimental measurement and showed a good agreement with the published literature.

8.5 Results and Discussion

All models with both aging effect and stenosis cases were used to study the airflow patterns and particle transport based on two variable conditions that are inlet velocities and particle sizes. In terms of initial velocities, this report will focus on three different inlet velocities that are 0.4915 m/s, 0.9829 m/s, and 1.9658 m/s as flow rate 7.5 lpm, 15 lpm, and 30 lpm respectively. In terms of particles sizes, this report will employ four different sizes that are 1 µm, 2.5 µm, 5 µm, and 10 µm.

8.5.1 Effects of Aging Cases

8.5.1.1 Airflow Analysis

Velocity Profiles

The velocity profiles will be located at seven different cross-sections on three different asymmetric lung models under the particle size of 10 µm. The comparison will be based on three different flow rates that are 7.5 lpm, 15 lpm, and 30 lpm. Figure 8.4 shows the velocity profiles for normal asymmetric lung whereas Figure 8.5 and 8.6 are the representative of the velocity profiles for the reduction of diameter by 10% and 20% respectively.

- *Velocity Profiles for asymmetric lung model*

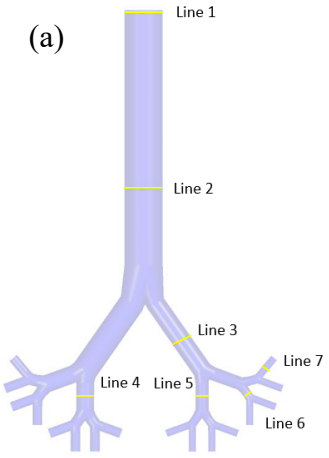

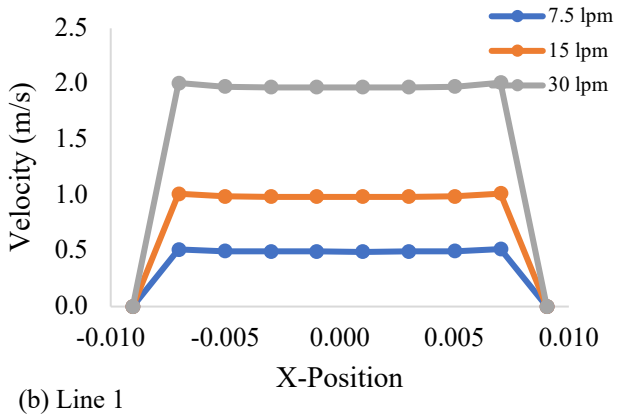

(b) Line 1

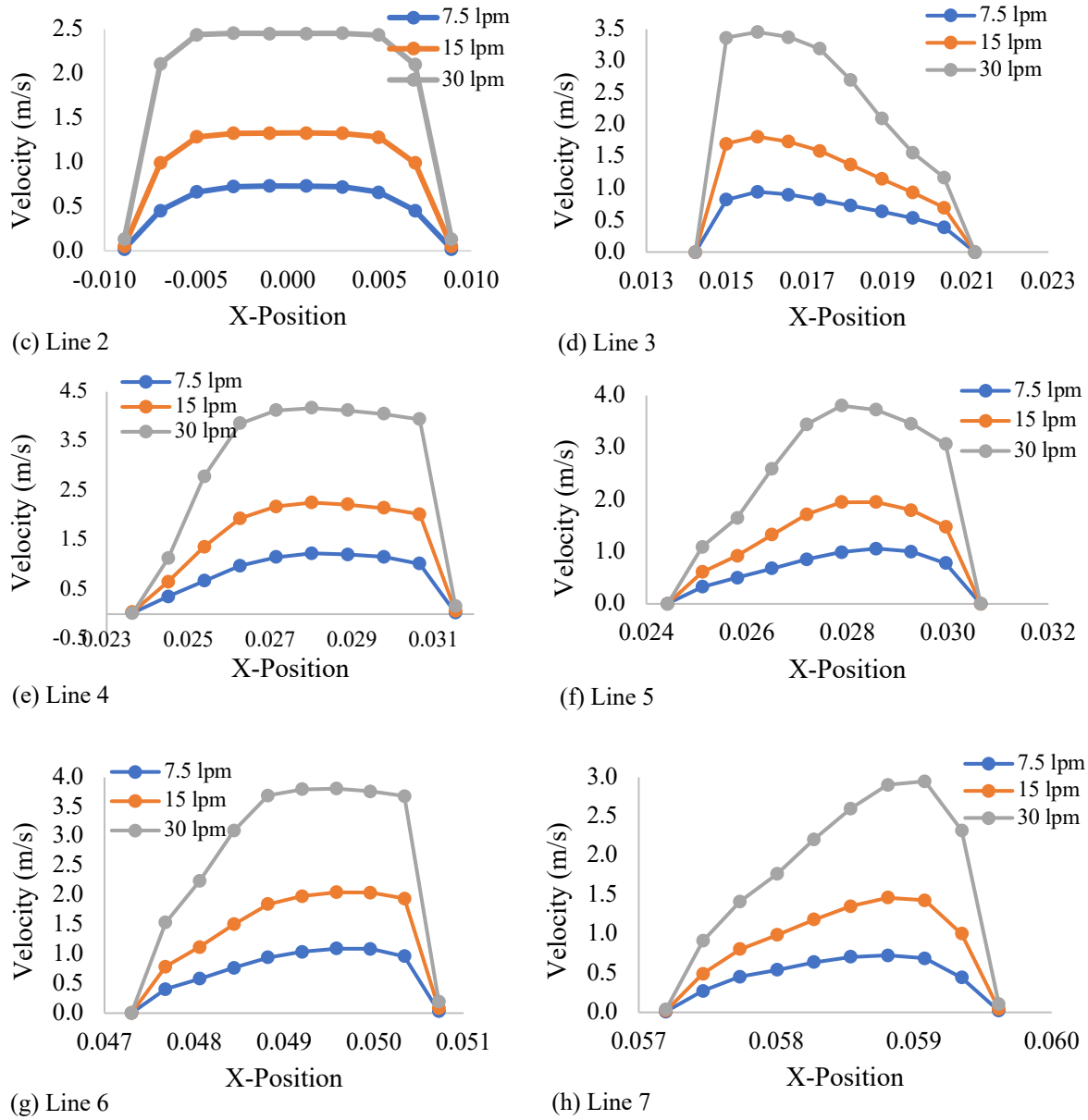

Figure 8.4 Selected line for velocity profiles of asymmetric lung model: (a) Selected location (b) Line 1, (c) Line 2, (d) Line 3, (e) Line 4, (f) Line 5, (g) Line 6, and (h) Line 7

Overall, in Figure 8.4, the velocities are continually increasing from the inlet and continually decreasing after through the airway at 3rd generation. The maximum velocity magnitude is at *Line 4* where it is the airway from the left-lung.

- *Velocity Profiles for asymmetric lung model with diameter reduction of 10%*

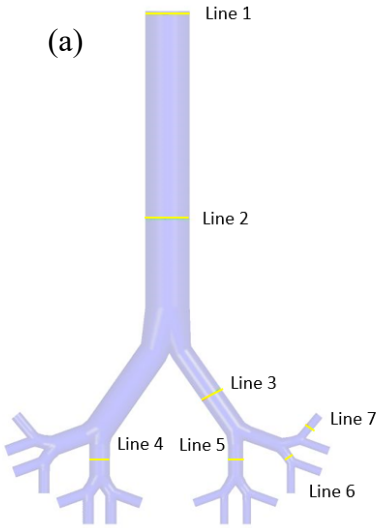

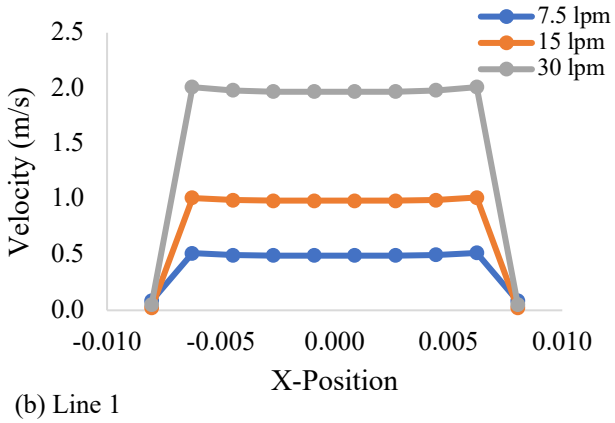

(b) Line 1

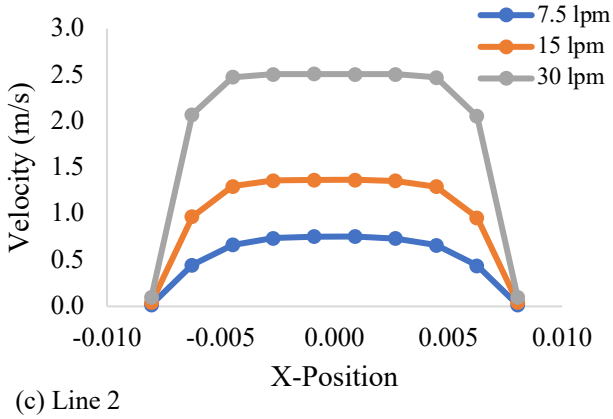

(c) Line 2

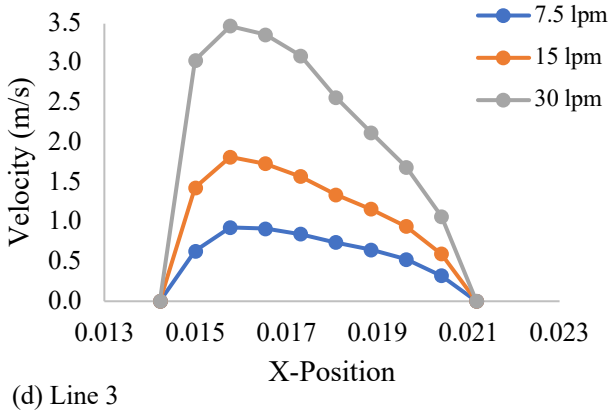

(d) Line 3

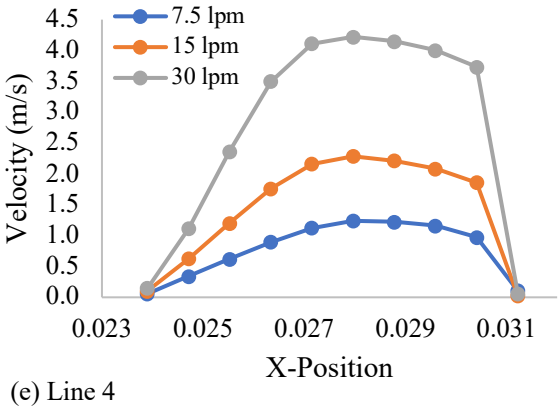

(e) Line 4

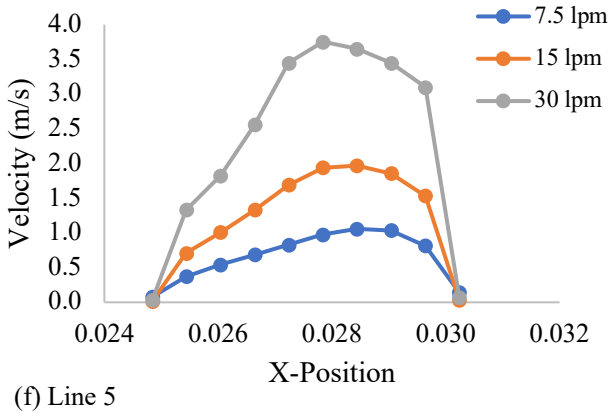

(f) Line 5

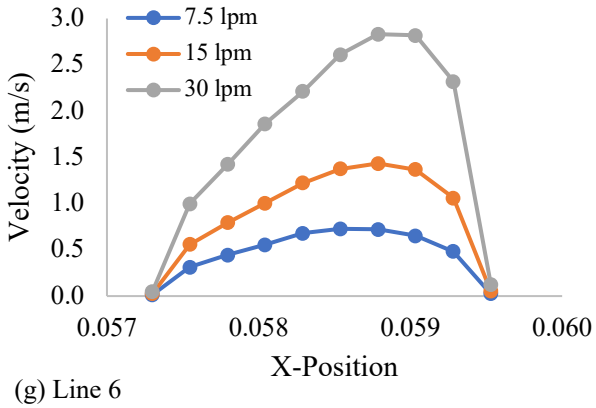

(g) Line 6

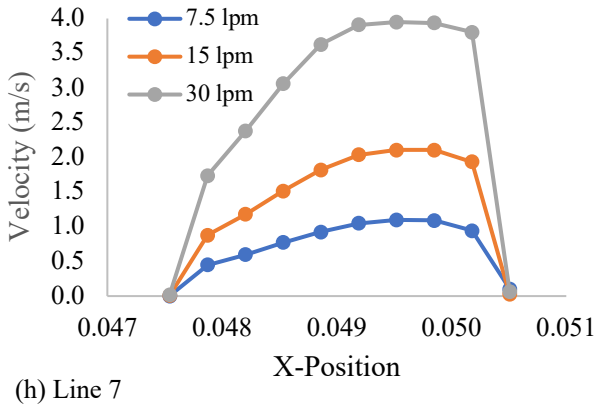

(h) Line 7

Figure 8.5 Selected line for velocity profiles of asymmetric lung model with diameter reduction of 10%: (a) Selected location (b) Line 1, (c) Line 2, (d) Line 3, (e) Line 4, (f) Line 5, (g) Line 6, and (h) Line 7

From above Figure 8.5, the velocities tend to continually increase from the inlet at trachea area to 2nd generation of the lung airways. However, after through 2nd generation, the velocities tend to decrease then becomes to increase again at 3rd and 4th generations, respectively. The maximum velocity magnitude is found at the airway from the left lung (Line 4) where it has a larger lung scale.

- *Velocity Profiles for asymmetric lung model with a diameter reduction of 20%*

(a)

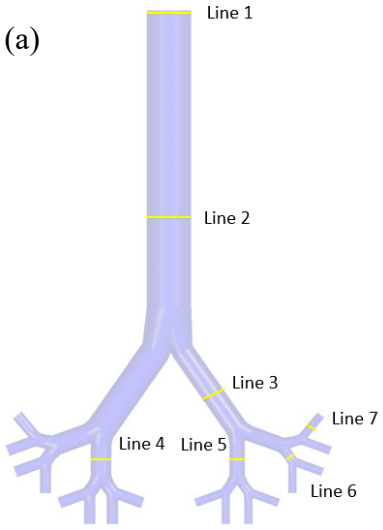

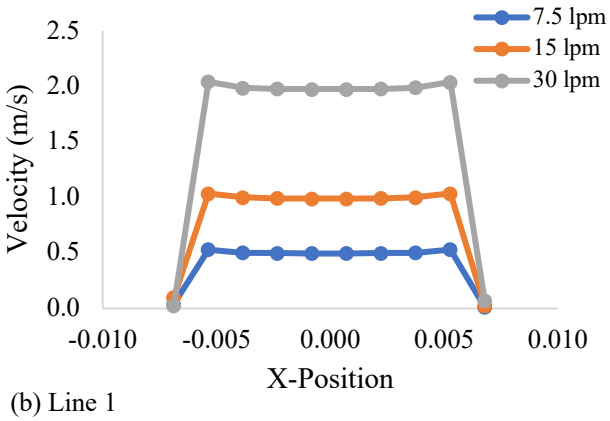

(b) Line 1

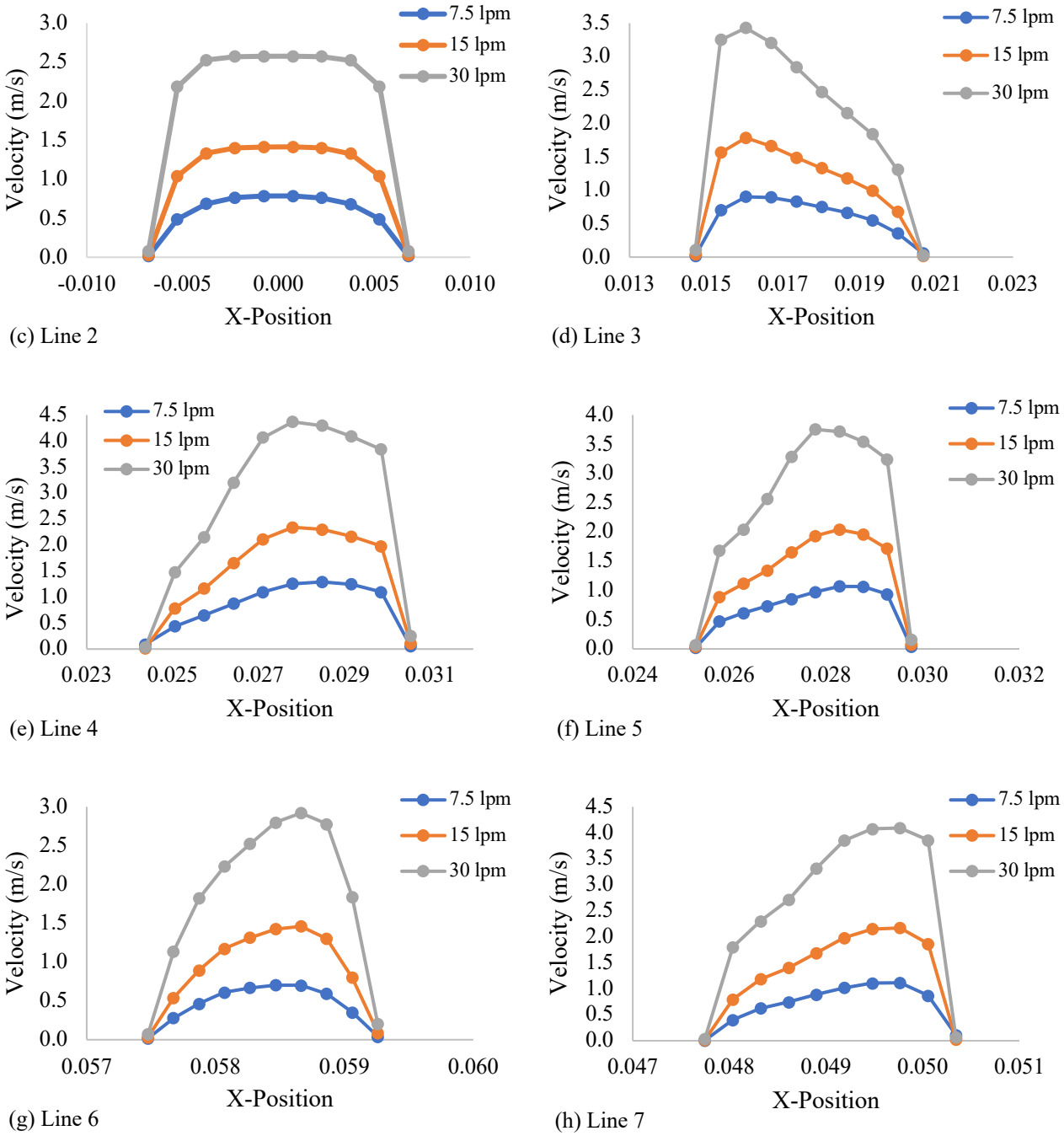

Figure 8.6 Selected line for velocity profiles of asymmetric lung model with diameter reduction of 10%: (a) Selected location (b) Line 1, (c) Line 2, (d) Line 3, (e) Line 4, (f) Line 5, (g) Line 6, and (h) Line 7

From Figure 8.6, the velocities tend to continually increase beginning from the inlet at trachea through 1st and 2nd generations. After that, the velocities seem to decrease at 3rd generation and return to increase at 4th generation. The maximum velocity magnitude is seen at the left-lung (Line 4) that has a larger diameter.

Overall, of velocity profiles from three different cases that have various lung volumes

(Figure 8.4 to Figure 8.6), the diameter of the whole lung airway could have a significant effect on the velocity patterns. The velocity tends to continually increase from the inlet at trachea to 2nd generation. After that, velocity decreases at 3rd generation and becomes increasingly again at 4th generation. In addition, the higher velocity usually occurs at the left-lung where it has a larger diameter. Based on the studies from Islam et al. (2017b); Singh et al. (2020), due to the airflow resistance of smaller airways, it can flow the air to the opposite lung side. In order to support this theory, the velocity magnitude from the reducing diameter cases have higher values as compared to normal lung case. By the diameter reduction of 20% has a maximum velocity magnitude and the diameter reduction of 10% has a second maximum velocity value.

Velocity Contours

There are two types of velocity contours that will be presented in this report. The first type is velocity contour for the whole domain on the XY plane whereas the second type is the contours at the cross-section planes. Figure 8.7 is the velocity contours for the asymmetric lung with having different diameters. Figure 8.7a is for normal asymmetric lung whereas Figure 8.7b, c is for the reduction of diameter by 10% and 20% respectively.

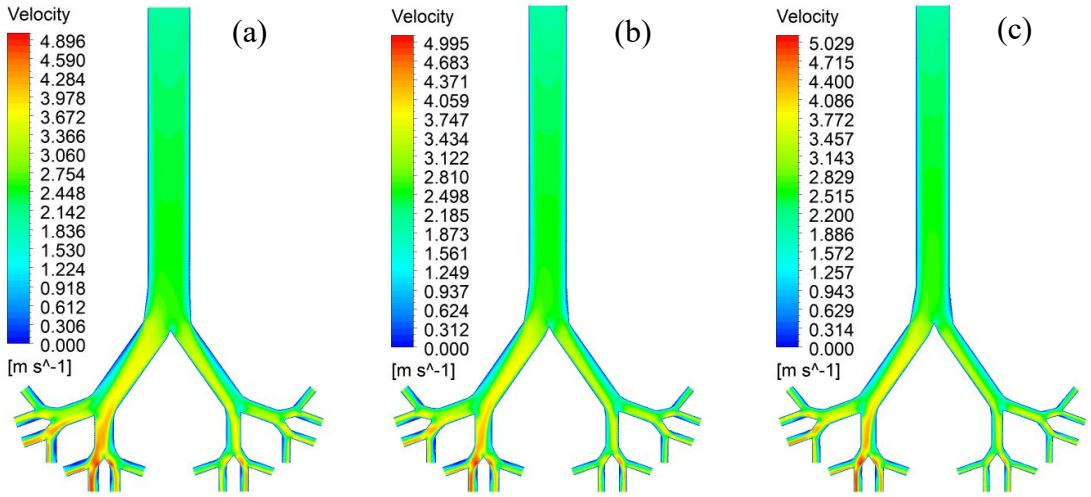

Figure 8.7 Velocity Contours at XY Plane for three lung models: (a) normal asymmetric lung, (b) reduction of diameter for 10%, (c) reduction of diameter for 20%.

Similar to the comparison from velocity profiles, the airflow velocity continually increases from the inlet at the trachea area. From Figure 8.7, all three cases have similar velocity patterns that have a higher velocity magnitude at the left-lung, where it is bigger than the right-lung. However, the maximum velocity magnitude tends to be found in the case that has 20% of the diameter reduction (Figure 8.7c) whereas the normal lung case (Figure 8.7a) has the lowest value

The selected planes are located at the random position which begins at trachea (0 generation) to 4th generation based on cross-sectional contours. The objective of these contours is to compare the level of velocity between the normal asymmetric lung and the lung that having smaller diameter with 10% and 20% of the diameter reduction. Figure 8.8 shows the location of selected planes at different generations. Figure 8.9 is the velocity contours for all three cases at different locations.

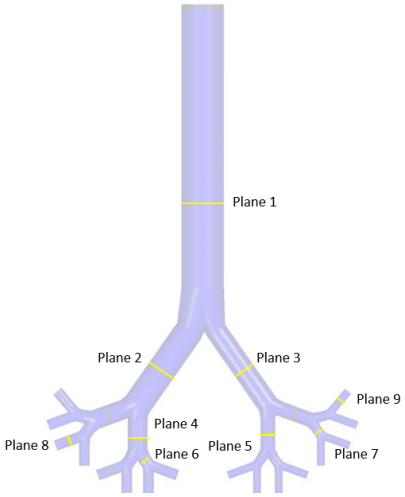

Figure 8.8 Selected planes for different positions of asymmetric lung models

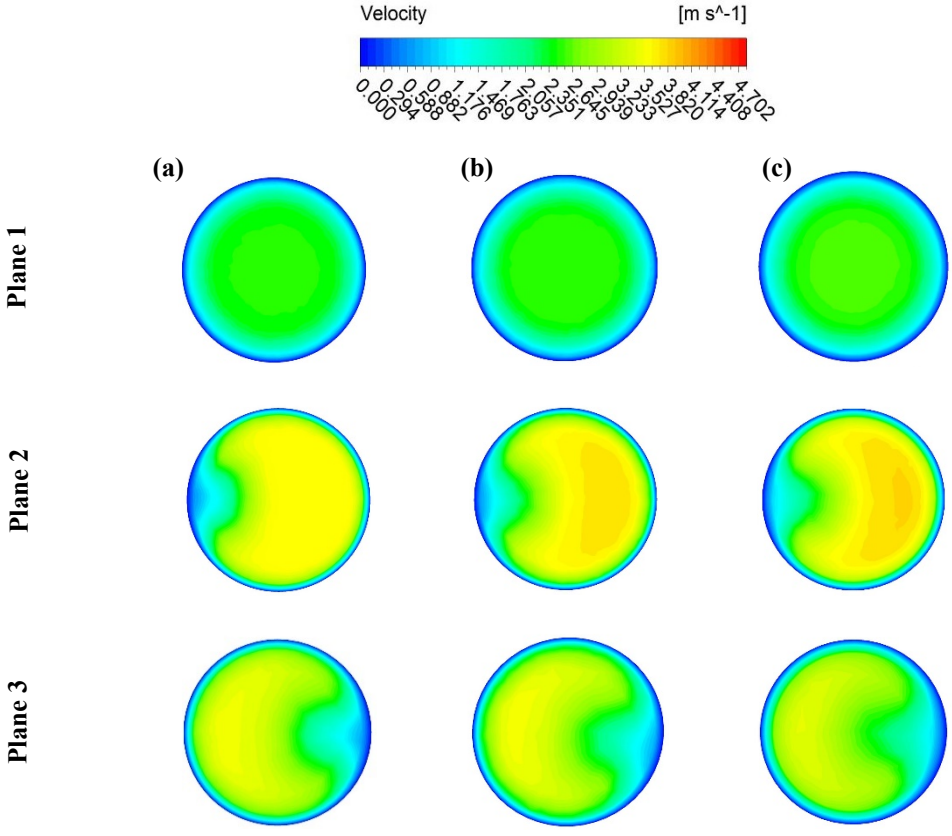

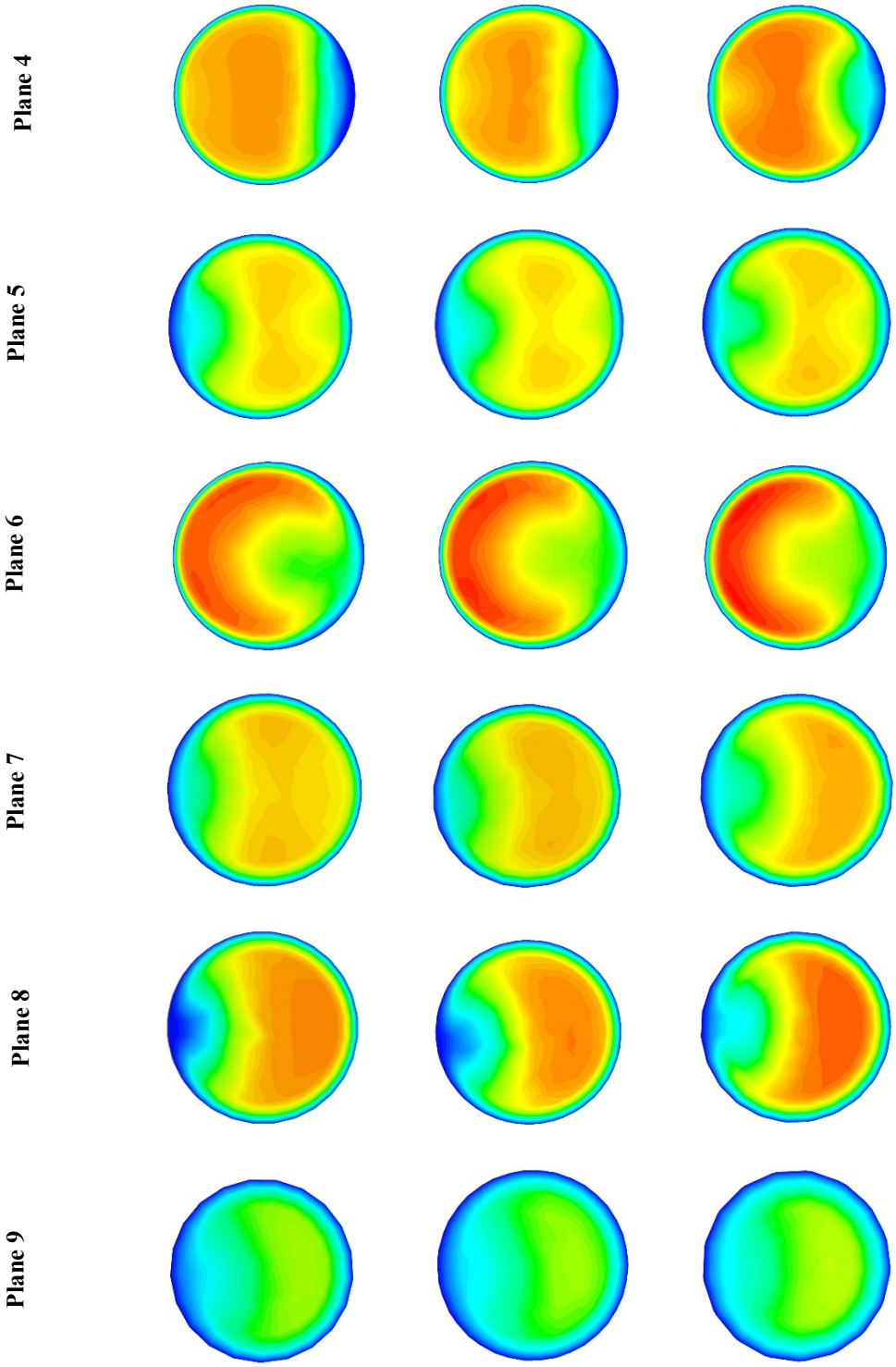

Figure 8.9 Velocity contours at different positions of asymmetric lung models at 30 lpm: (a) normal asymmetric lung, (b) reduction of diameter for 10%, (c) reduction of diameter for 20%.

From Figure 8.9, the velocity contours at trachea area (*Plane 1*) are found to be similar for all three cases. Similarly, the velocity contours at 1st generation (*Plane 2* and *3*) and other generations (*Plane 4* to *Plane 9*) also tend to be similar for all three cases. However, the higher

and highest levels are usually found at the left-lung airways that having larger diameter (*Plane 4, 6, 8*). According to Singh et al. (2020), the velocity pattern of velocity contour can be changed by the shape of airways conditions. Therefore, the maximum velocity magnitude for each plane belongs to the smallest airway (Figure 8.9c).

8.5.1.2 Pressure Drop

The pressure drop and pressure contours are presented in this section.

Pressure Drop

The randomly selected planes are firstly located in the middle of the trachea through the whole lung to 4th generation. The calculation for pressure drop is based on 10 µm of particle size and three different flow rates that are 7.5 lpm, 15 lpm, and 30 lpm. Figure 8.10 presents the pressure drop at nine selected planes for three cases.

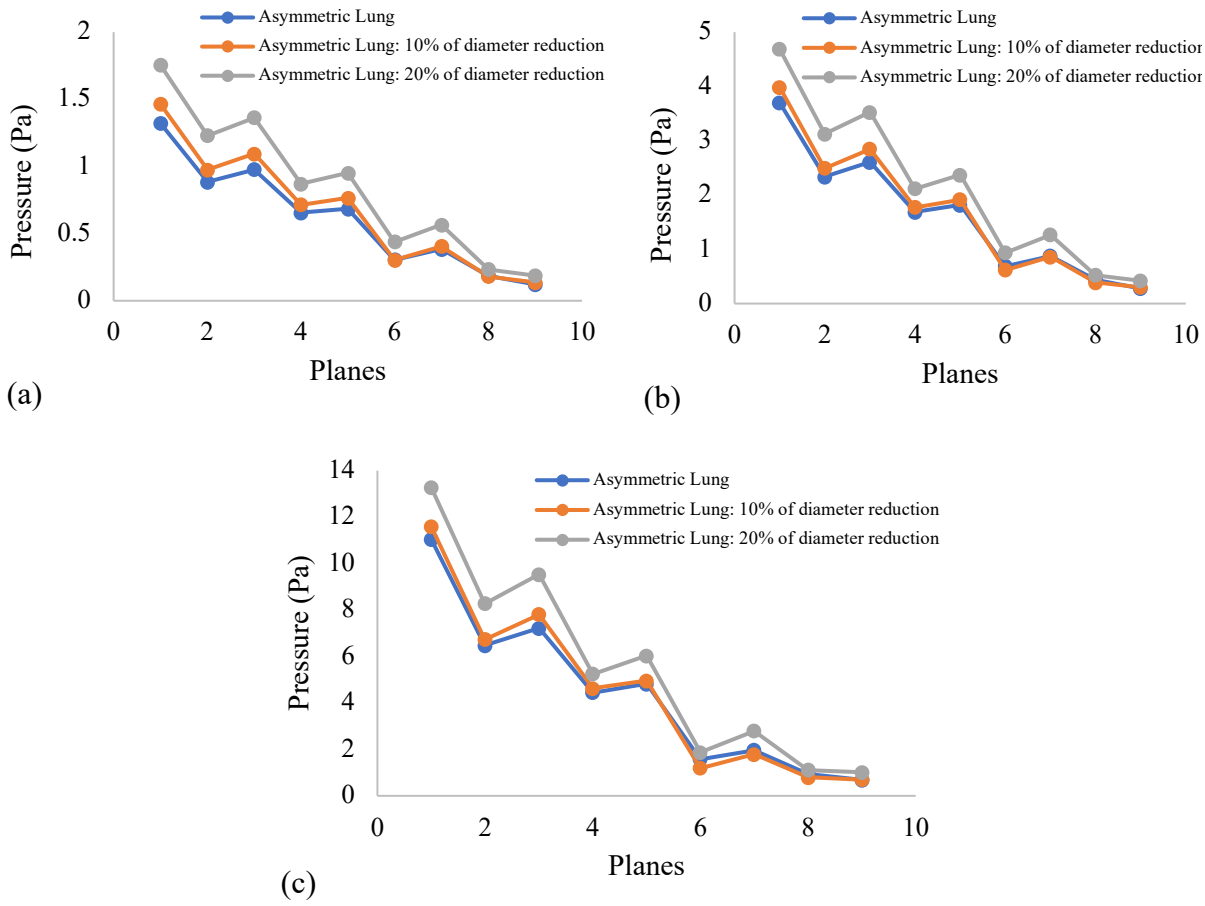

Figure 8.10 Pressure drop at different plane positions for asymmetric lung with different diameters: (a) 7.5 lpm, (b) 15 lpm, and (c) 30 lpm.

The results from Figure 8.10 indicate that the pressure continually decreases from the inlet

because of the air direction that always flows from the higher-pressure area to the lower-pressure area. The maximum pressure drop is found at the lowest branch at 4th generation (*Plane 9*) for the highest flow rate at 30 lpm (Figure 8.10c). In terms of maximum pressure, the case, which has the smallest diameter, usually has maximum pressure at the inlet as compared to another two cases.

To summarize, the level of pressure drop tends to be based on the flow rate. A higher flow rate can cause higher pressure and a higher pressure drop. In terms of the effect of the diameters for the whole lung, the case, which has a diameter reduction of 10%, has a similar pressure level to the normal lung case. On the other hand, 20% of diameter reduction case has a higher pressure level than another two cases.

Pressure Contours

The overall of pressure for the whole lung model is provided based on the XY Plane of the contours feature. Highest flow rates (30 lpm) and largest particle size (10 µm) were used for the simulation. Figure 8.11 indicates the pressure contour at XY Plane for three different diameters.

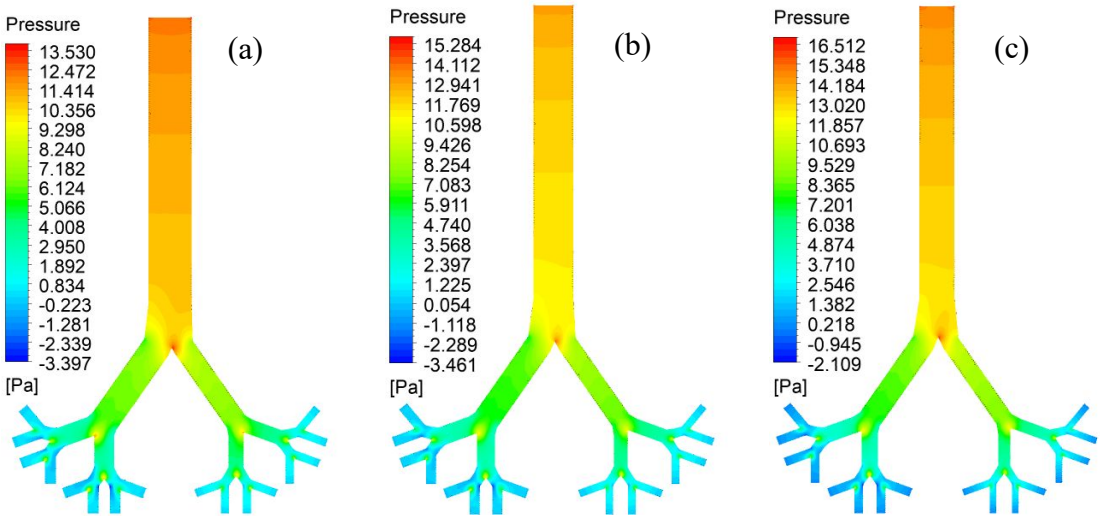

Figure 8.11 Pressure Contours at XY Plane for three lung models: (a) normal asymmetric lung, (b) reduction of diameter for 10%, (c) reduction of diameter for 20%.

From Figure 8.11, all three cases have similar patterns in terms of the level of the pressure. The pressure tends to continually decrease from the inlet at trachea to other generations. However, a higher pressure always occurs at the bifurcation for all generations. Furthermore, the highest pressure is generally located at the bifurcation of the 1st generation for all three cases. It can be noticed that the case that has the smallest diameter has the highest range of pressure (Figure 8.11c). Referring to Nowak et al. (2002), lung volume can lead to different pressure levels in

bifurcation. It can be summarized that a smaller diameter will lead to a higher pressure level.

8.5.1.3 Wall Shear

The shear stress at the wall is obtained based on the calculation with the flow rate of 30 lpm and particle diameter of 10 µm. Figure 8.12 shows the shear stress at the wall for normal asymmetric lung and two of diameter reductions.

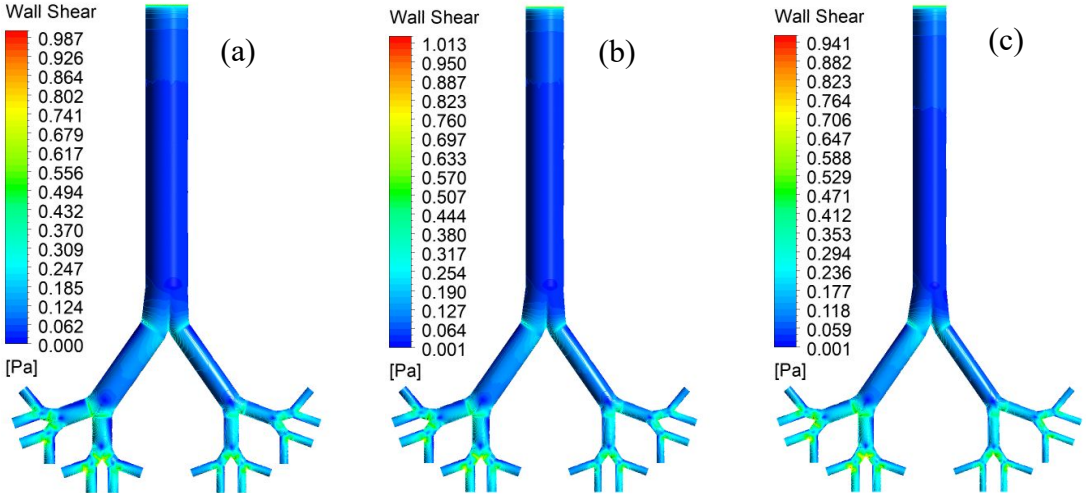

Figure 8.12 Wall shear for three lung models at 30 lpm: (a) normal asymmetric lung, (b) reduction of diameter for 10%, (c) reduction of diameter for 20%.

Figure 8.12 indicates that the shear stress at the wall is higher at the inlet area for all three cases. Then, it decreases and begins to increase again after passing 1st generation of the airway. The higher shear stress is always found in the bifurcation area for all cases. However, the highest shear stress is found at the case which has 10% reduction of diameter (Figure 8.12b), whereas the secondary highest shear stress belongs to the normal lung case (Figure 8.12a). Consequently, the level of shear stress at the wall is slightly influenced by the airway volume and has a greater influence from the bifurcation area.

8.5.1.4 Turbulent Intensity

In this section, the comparison of the level of turbulent intensity for three different cases is provided based on the 30 lpm of the flow rate and 10 µm of the particle size. Figure 8.13 presents the turbulent contour for the whole lung with three different cases.

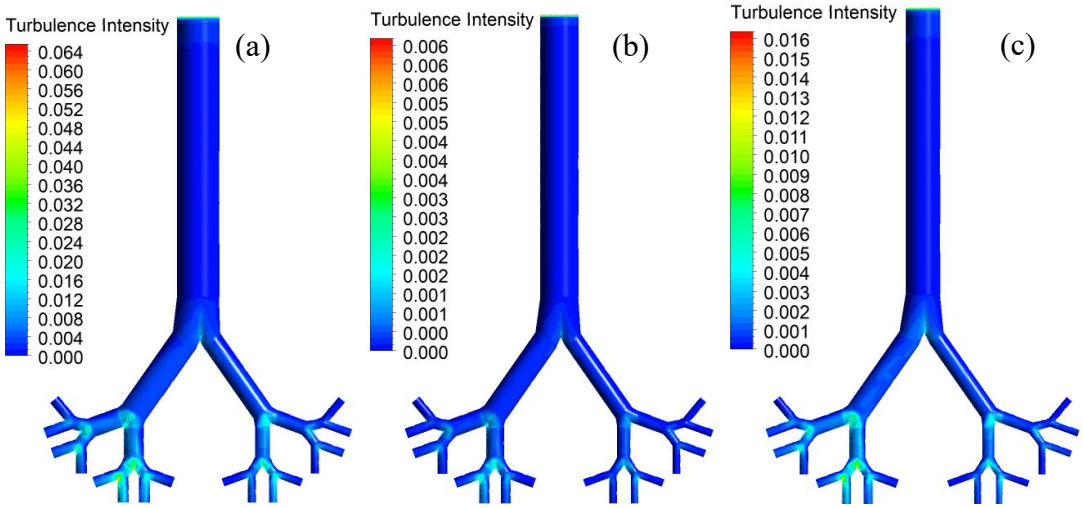

Figure 8.13 Turbulence intensity contour for three lung models at 30 lpm: (a) normal asymmetric lung, (b) reduction of diameter for 10%, (c) reduction of diameter for 20%.

From Figure 8.13, turbulent flow is observed at the inlet region and at the bifurcation area for each generation. It can be seen that turbulence intensity occurs at the same location for both normal lung case and the 20% reduction of diameter case (Figure 8.13a, c), whereas the second case (Figure 8.13b) has differently turbulent occurring. This case only has turbulence intensity at 4th bifurcation of left-lung. To compare three cases that have different diameters, the highest turbulence intensity is located in the first case (Figure 8.13a) that has a normal diameter. However, there is only a slight variation of turbulence intensity from all three cases. Therefore, it can be summarized that the diameter could have an insignificant effect on the level of turbulence intensity.

Turbulent intensity at a different position is calculated based on nine selected planes which involve 0 generation to 4th generation. The flow rate at 30 lpm is used for the calculation of three different lung models, as shown in Figure 8.14.

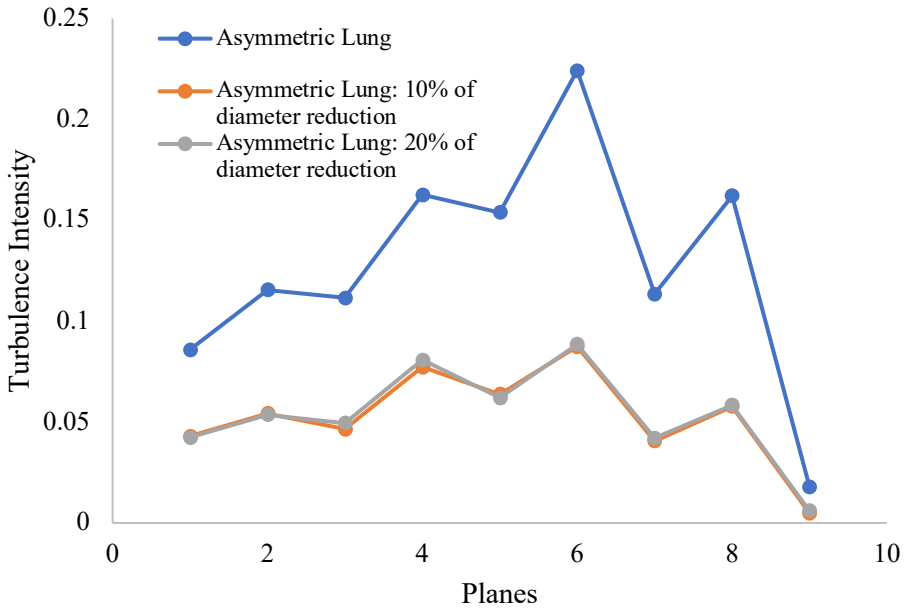

Figure 8.14 Turbulence intensity at different plane positions for three lung models at 30 lpm

From the graph of Figure 8.14, it can be seen that the normal lung airway has a greater amount of turbulence intensity. The highest turbulence fluctuation also occurs at Plane 6 where it is located at 3rd generation. Both cases that have the diameter reducing conditions have totally the same trends. However, the airflow becomes to be stable at the 4th generation and tends to be continually stable for all lower generations.

8.5.1.5 Particle Transport

Deposition Efficiency

The comparison of particle deposition efficiency for asymmetric lung model with having different sizes is presented based on the three different flow rates that are 7.5 lpm, 15 lpm, and 30 lpm (showing at Figure 8.15).

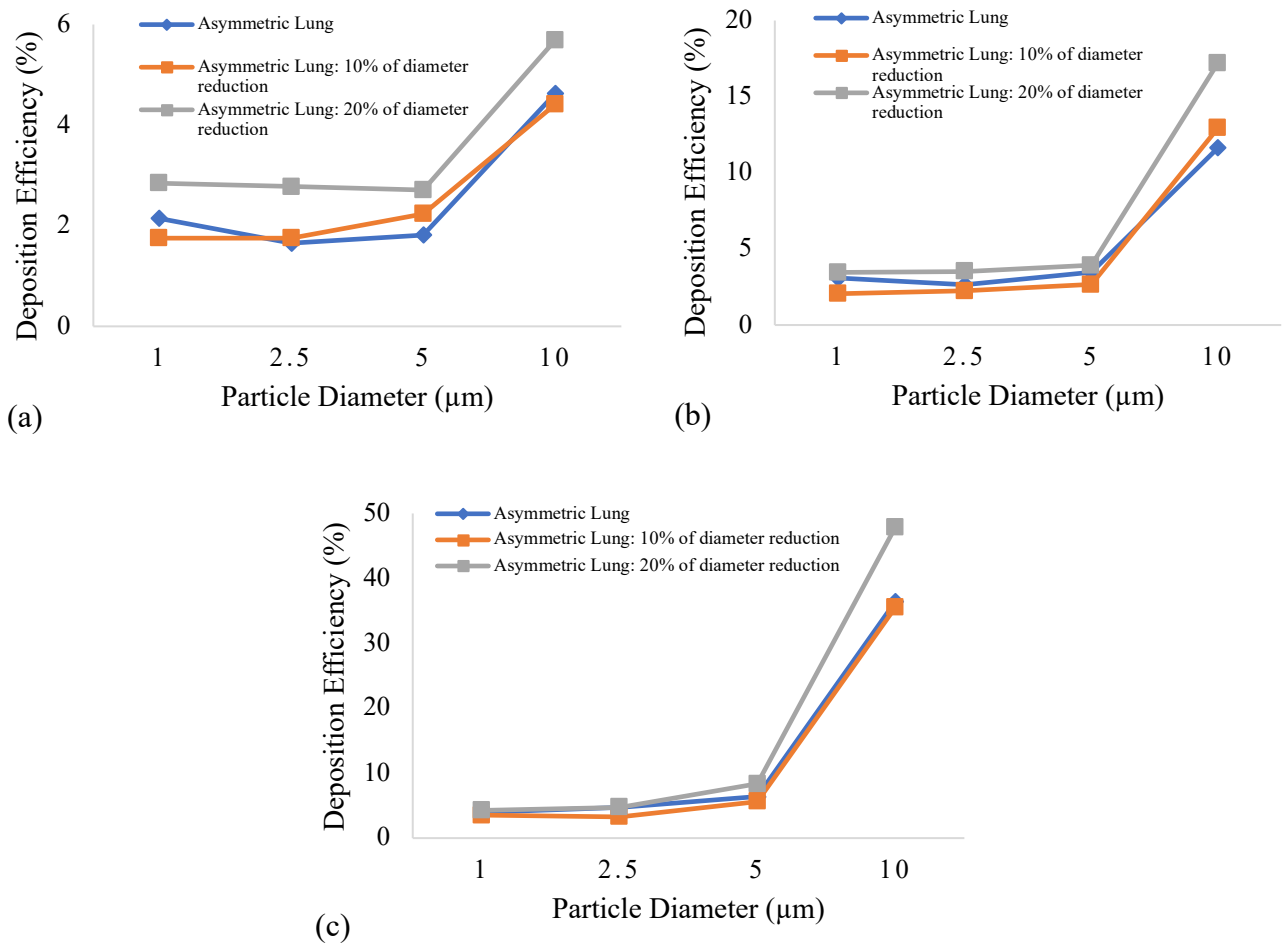

Figure 8.15 Deposition Efficiency in different regions of asymmetric lung for three different diameters: (a) 7.5 lpm, (b) 15 lpm, and (c) 30 lpm.

From Figure 8.15, it is clear that the airway volume can significantly affect deposition efficiency. Smallest lung airways have a greater amount of particle deposition for all flow rates whereas another two lungs, that have bigger diameters, have similar levels. One of the key factors that could influence the level of particle efficiency is the flow rate. If compared to all flow rates from above figure, the highest flow rate that is 30 lpm (Figure 8.15c) has the highest deposition efficiency which reaches around 48% in terms of 10 µm of particle size whereas the flow rates at 7.5 lpm and 15 lpm (Figure 8.15a, b) could reach around 6% and 17% respectively. It can be summarized that a higher particle inertia, which is caused by larger particle size and higher flow rate, could increase the deposition efficiency (van Ertbruggen et al. 2004; Ma & Lutchen 2009; Singh et al. 2020). In addition, the diameter of the lung airways also affected the deposition efficiency rate especially for the case of having a 20% diameter reduction.

Deposition Fraction

The calculation of deposition fraction for different particle diameters is shown at Figure 8.16.

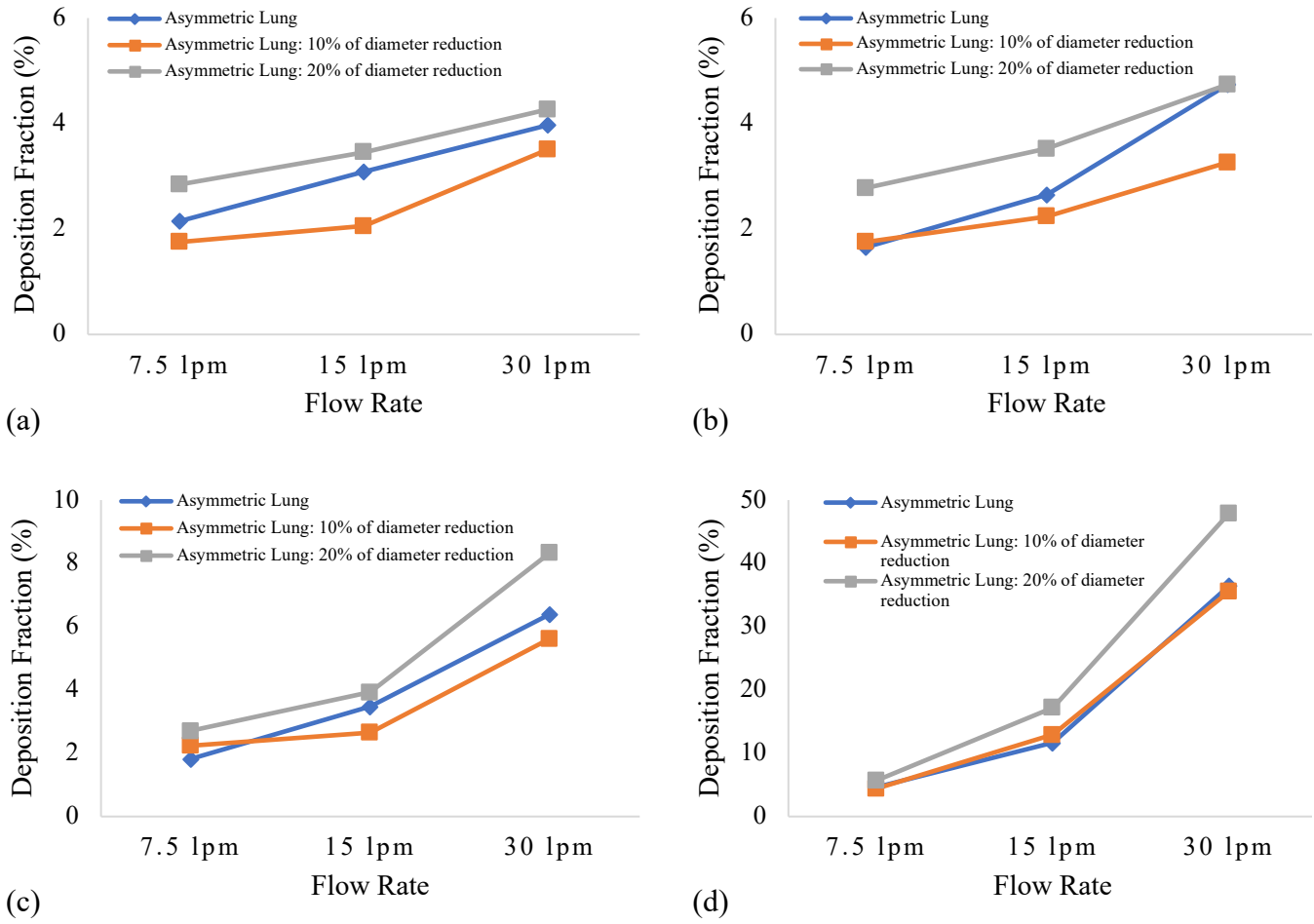

Figure 8.16 Deposition Fraction of different-diameter particles in asymmetric lung for three different diameters: (a) 1 µm diameter, (b) 2.5 µm diameter, and (c) 5 µm diameter, and (d) 10 µm diameter.

From Figure 8.16, the particle sizes as 1 µm and 2.5 µm (Figure 8.16a, b) have similar deposition fraction rates that are around 2% to 5% for all three flow rates, while the particle size as 5 µm (Figure 8.16c) has the range between 2% to 8% for all three flow rates. However, the largest particle size as 10 µm (Figure 8.16d) has the highest range between 6% to 48%. By the highest deposition fraction is found at the highest flow rate at 30 lpm. For the overall deposition fraction in case of having three different diameters of the lung airways, it can be seen that the smallest lung airway with 20% of diameter reduction usually has a higher deposition rate for all particle sizes whereas another two lung airways have slightly different deposition rates.

To summarize, the deposition fraction is generally based on the particle size, flow rate, and including density (Islam et al. 2015; Lalas et al. 2017; Singh et al. 2020). Larger particle size and higher flow rates can increase the deposition fraction. The airway volume can also influence the deposition fraction. However, it is only for the case of a 20% diameter reduction

while the case of a 10% diameter reduction has similar ranges to normal airways case.

Four different particle sizes are used to be the injection from the inlet at trachea area under the different diameter of three asymmetric lungs with the flow rate at 30 lpm. Figure 8.17 is the scenario of the particle deposition with three lung conditions.

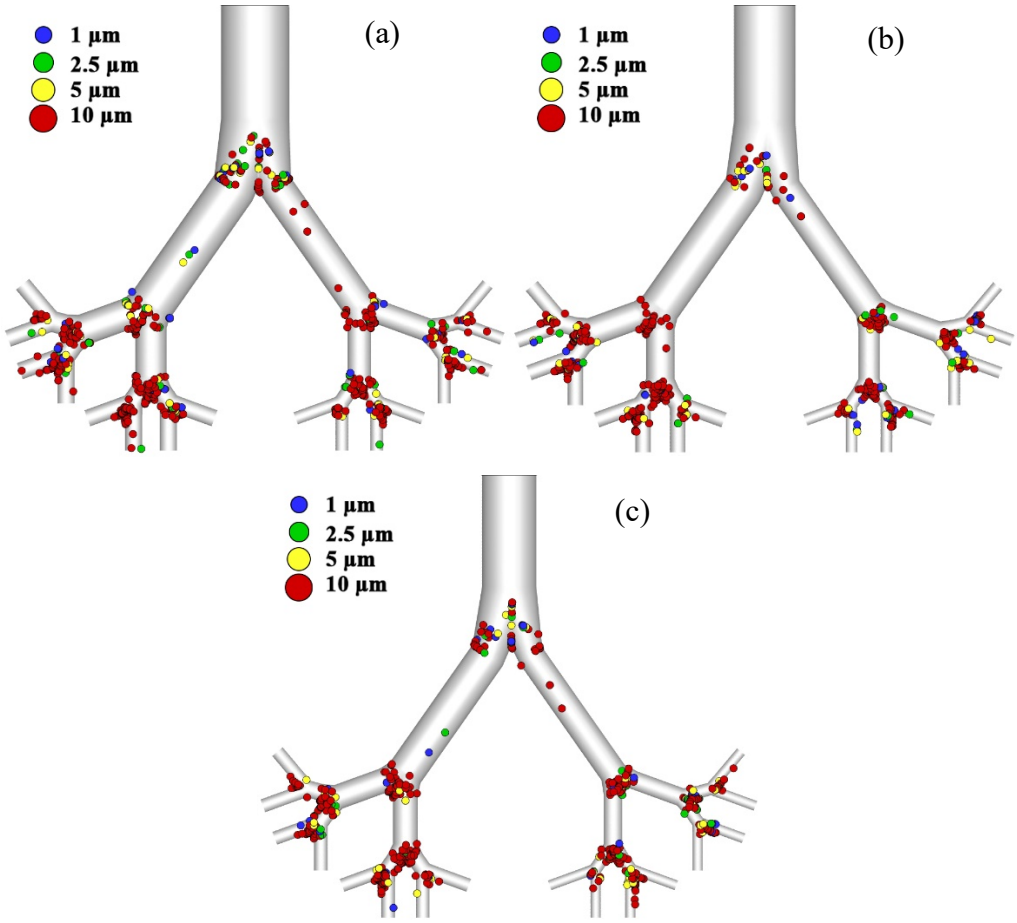

Figure 8.17 Particle deposition scenario at 30 lpm for three lung models: (a) normal asymmetric lung, (b) reduction of diameter for 10%, (c) reduction of diameter for 20%.

The overall of three cases, particles are usually trapped at the left-lung rather than right-lung because of having a higher lung volume. Most particles are trapped at the wall of a bifurcation for all generations (Balashazy& Hoffman 1995; Farghadan et al. 2019). It can be seen that after through the 1st generation, the particles as 10 µm seem to be deposited greater than other particle sizes. If compared to the deposition for all generations, particle size as 10 µm is likely trapped at the bifurcation of the 2nd generation whereas other particle sizes are slightly trapped at this generation. It can be summarized that the majority of particle sizes (10 µm) can be trapped in the lung airways from the 1st to 4th generations.

8.5.2 Stenosis Cases

8.5.2.1 Airflow Analysis

In order to understand the airflow characteristic, this report will provide a clear understanding of airflow patterns by considering two features that are velocity profiles and velocity contours.

Velocity Profiles

Velocity profiles, it can be classified as the variation in velocity on a line at the right angles to the original flow's direction. It could be the representative of the velocity magnitude and change of the flow direction caused by the various shapes within the domain. In other words, velocity profiles can represent flow's behavior during transportation through the domain.

In this section, the velocity profiles will be plotted at seven different cross-sections on the five different cases in asymmetric model with stenosis sections with 10 µm for the particle size. Figure 8.18 will be for the lung with stenosis area at 1st generation. Figure 8.19 and 8.20 will be for the airways with stenosis areas at 2nd generation in left and right lungs. Figure 8.21 and 8.22 will be for the geometry with stenosis areas at 3rd and 4th generations. In details, it can be easily described that *Line 1*will be the representative of the inlet, *Line 2* will be the middle of the trachea, *Line 3* will be for the right lung at 1st generation, and *Line 4* and *5* will be for the left-lung and right-lung at 2nd generation. In contrast, *Line 6* and *7* will be for the right-lung at 3rd and 4th generation respectively.

- *Velocity Profiles for asymmetric lung model with right-stenosis area at 1st generation*

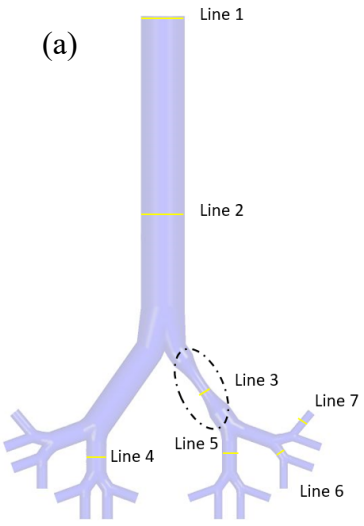

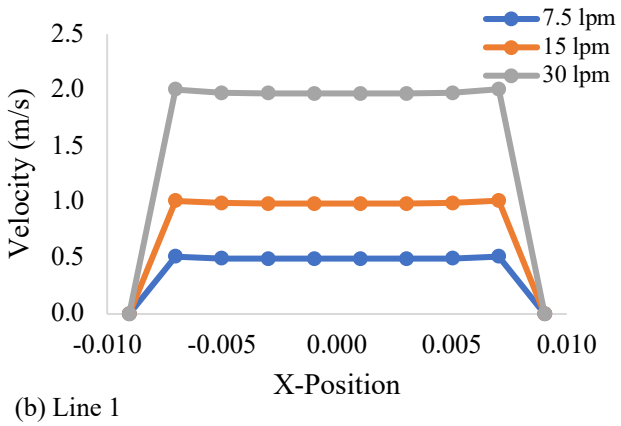

(b) Line 1

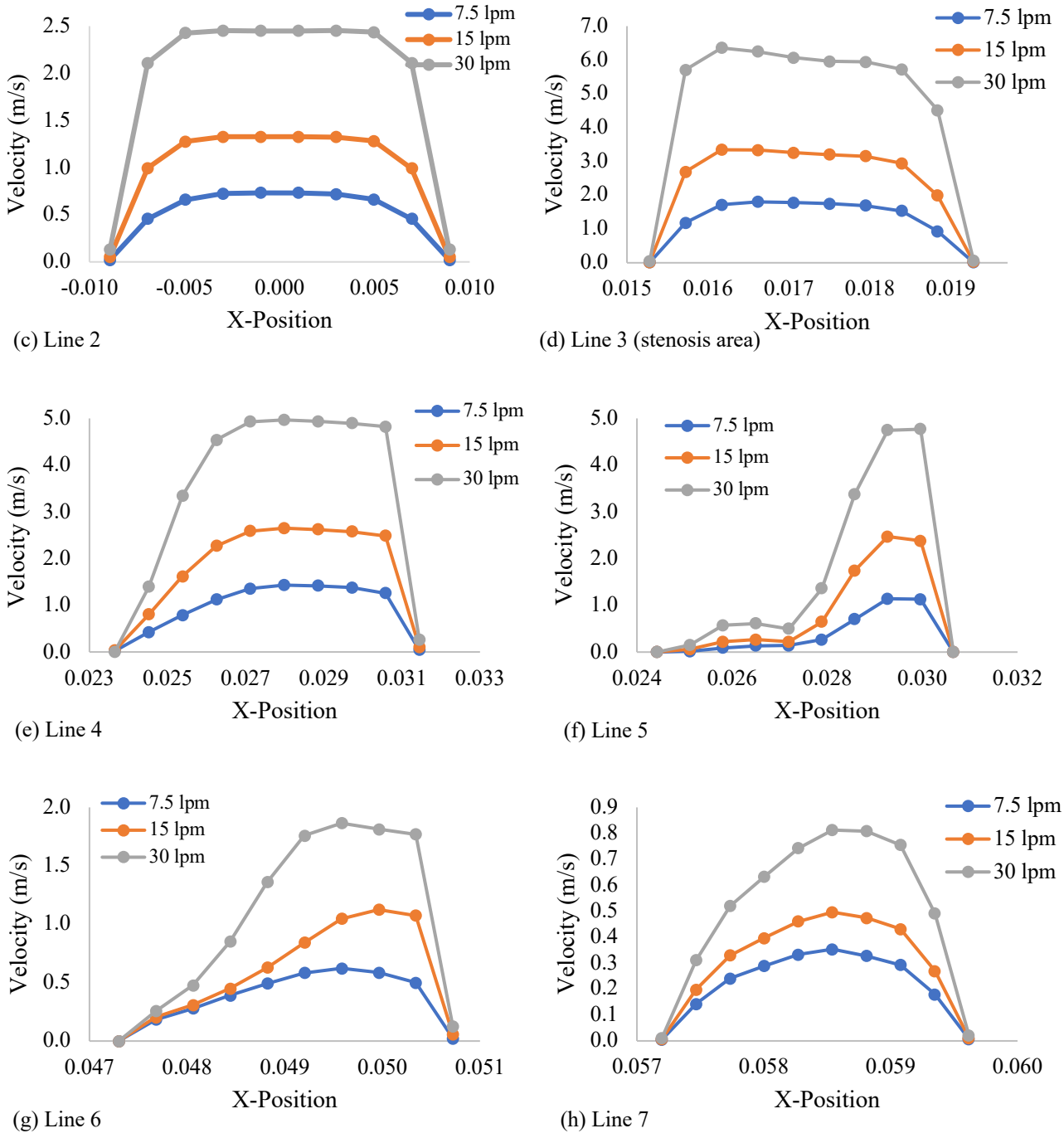

Figure 8.18 Selected line for velocity profiles of asymmetric lung model with stenosis area at 1st generation: (a) Selected location (b) Line 1, (c) Line 2, (d) Line 3 at stenosis area, (e) Line 4, (f) Line 5, (g) Line 6, and (h) Line 7

Overall, in Figure 8.18, the velocities are continually increasing from the inlet and becoming lower after through the stenosis region at 1st generation. The lowest velocity magnitude occurs in*Line 7* where it is located in the 4th generation. The maximum velocity magnitude is at *Line 3*, which is the stenosis area.

- *Velocity Profiles for asymmetric lung model with left-stenosis area at 2nd generation*

(a)

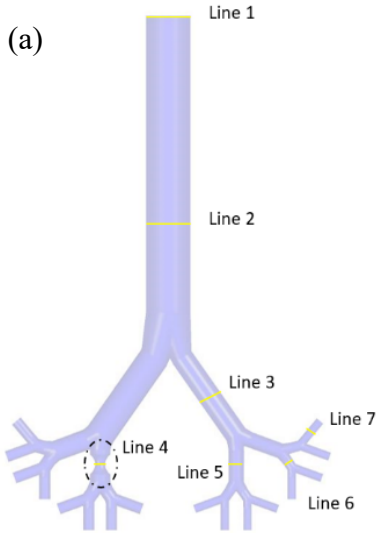

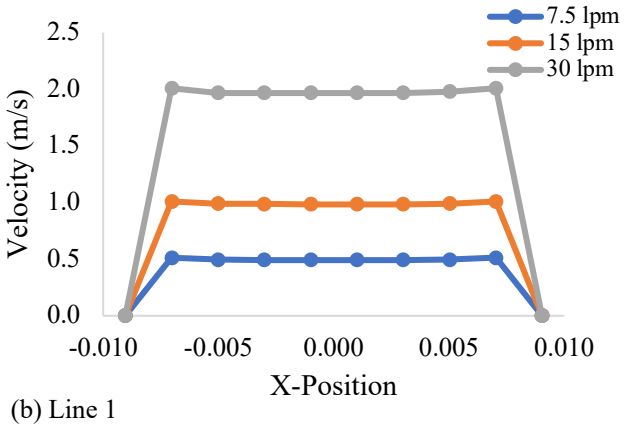

(b) Line 1

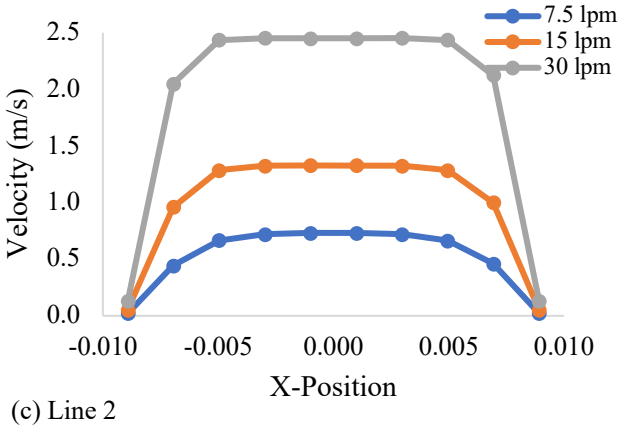

(c) Line 2

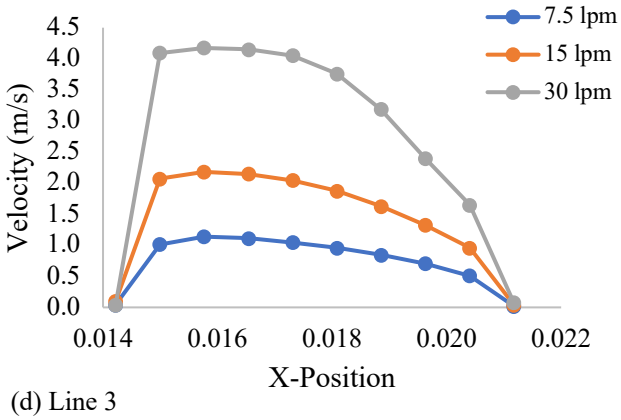

(d) Line 3

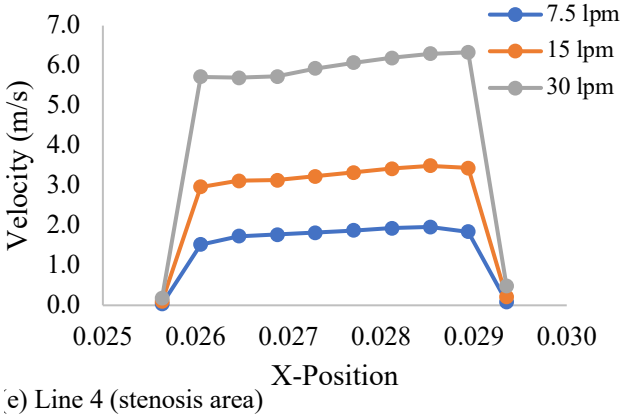

(e) Line 4 (stenosis area)

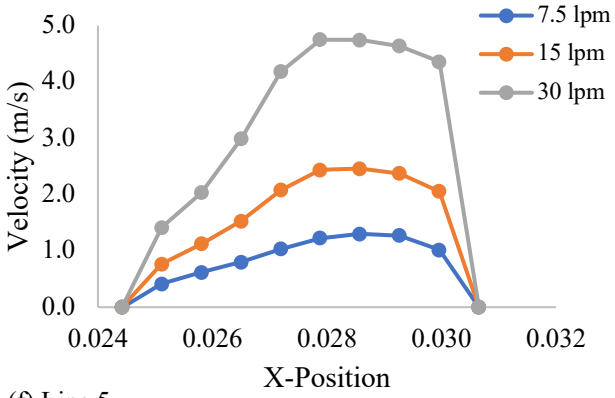

(f) Line 5

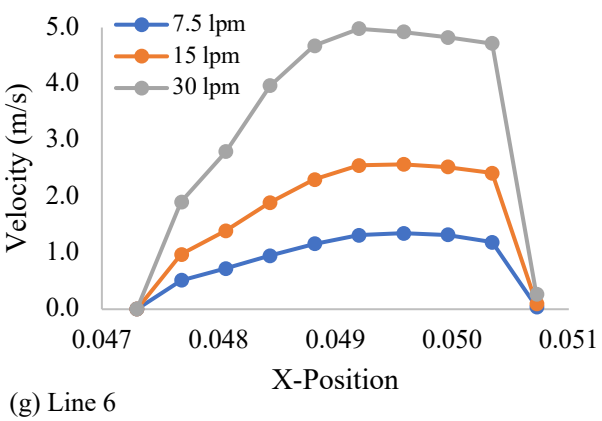

(g) Line 6

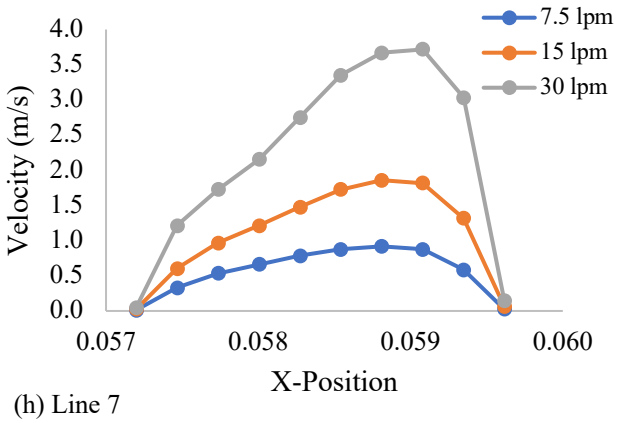

(h) Line 7

Figure 8.19 Selected line for velocity profiles of asymmetric lung model with left-stenosis area at 2nd generation: (a) Selected location (b) Line 1, (c) Line 2, (d) Line 3, (e) Line 4 at stenosis area, (f) Line 5, (g) Line 6, and (h) Line 7

Overall, in Figure 8.19, the velocities are continually increasing from the inlet and continually decreasing after through the airway at 3rd generation. The maximum velocity magnitude, in this case, occurs in the stenosis area (*Line 4*). It can be summarized that the velocity at the left-lung is higher than the right-lung.

- *Velocity Profiles for asymmetric lung model with right-stenosis area at 2ndgeneration*

(a)

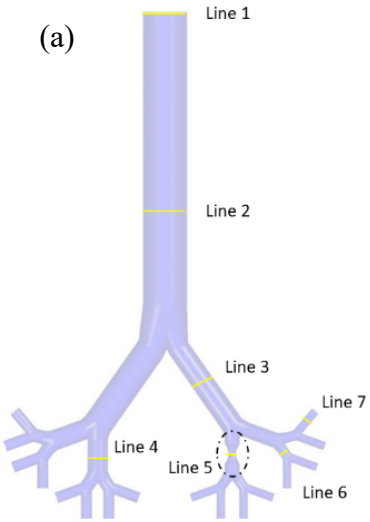

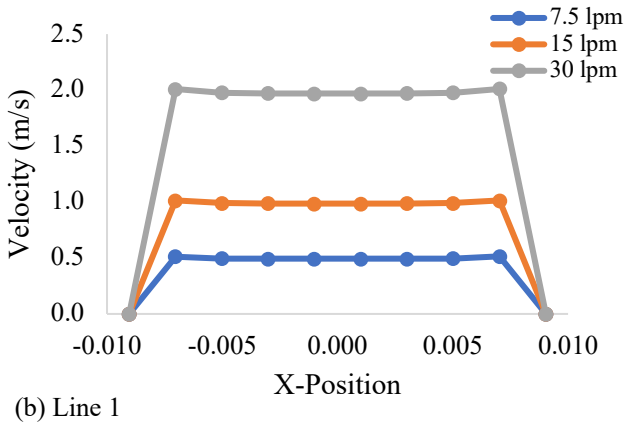

(b) Line 1

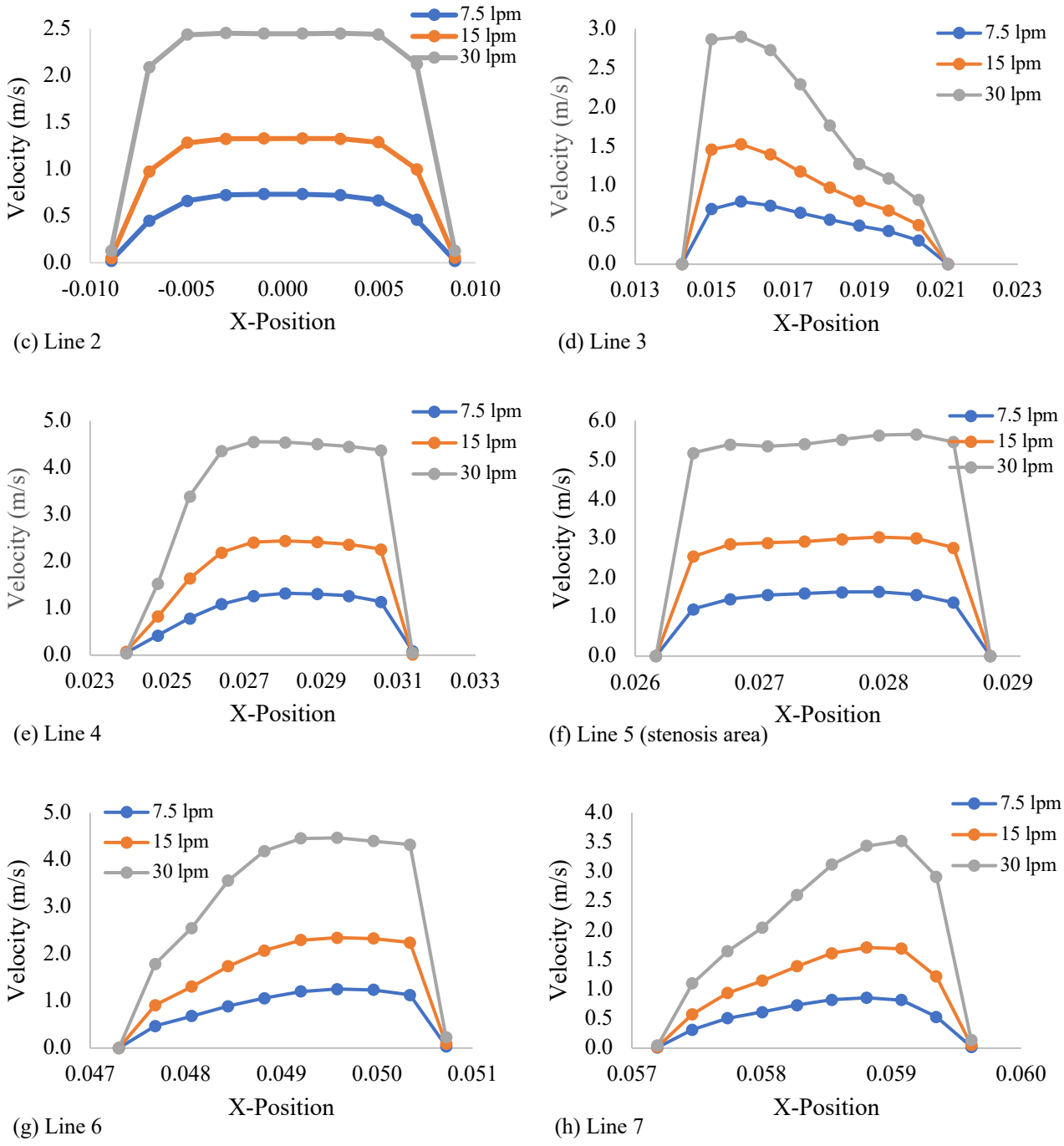

Figure 8.20 Selected line for velocity profiles of asymmetric lung model with right-stenosis area at 2nd generation: (a) Selected location (b) Line 1, (c) Line 2, (d) Line 3, (e) Line 4, (f) Line 5 at stenosis area, (g) Line 6, and (h) Line 7

Overall, in Figure 8.20, the velocities are continually increasing from the inlet and becoming decreasing from 3rd generation. The maximum velocity magnitude occurs in the stenosis area (*Line 5*), where it is in the 2nd generation.

- *Velocity Profiles for asymmetric lung model with right-stenosis area at 3rd generation*

(a)

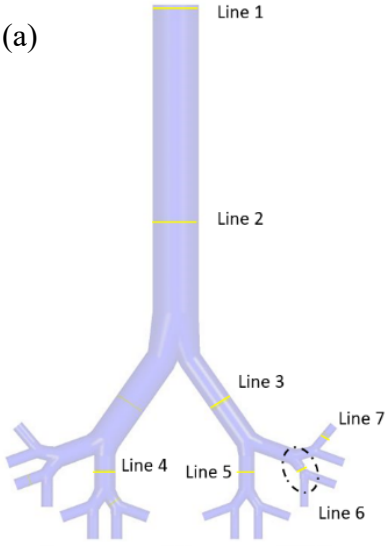

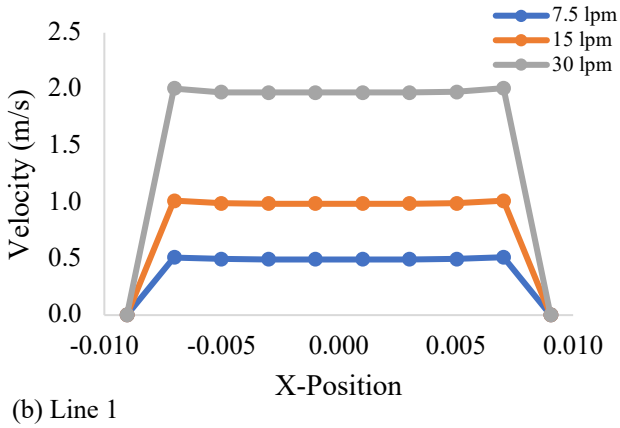

(b) Line 1

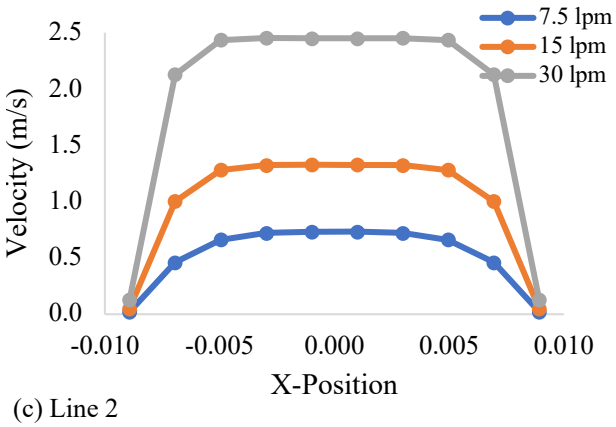

(c) Line 2

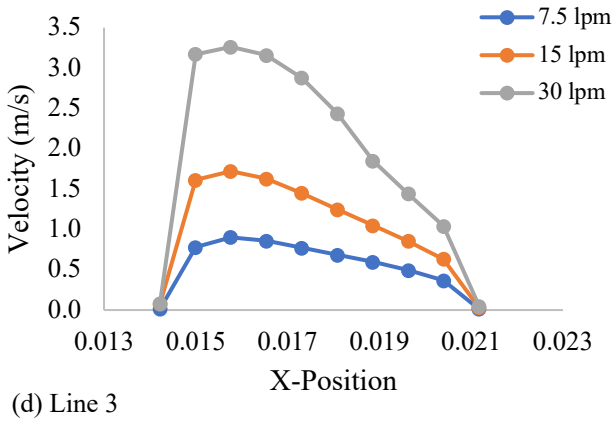

(d) Line 3

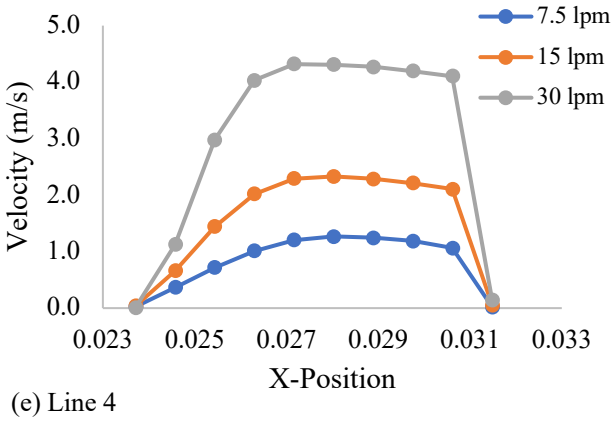

(e) Line 4

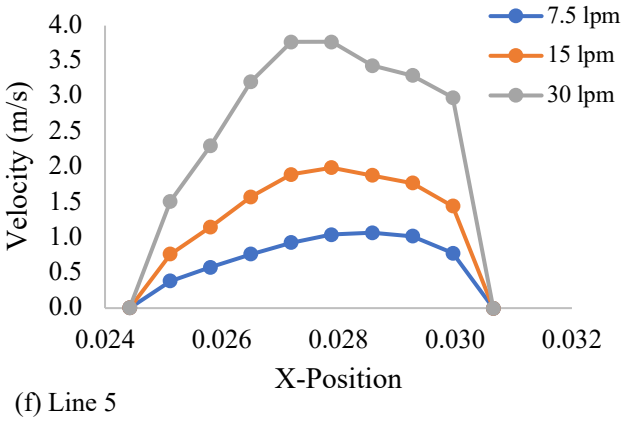

(f) Line 5

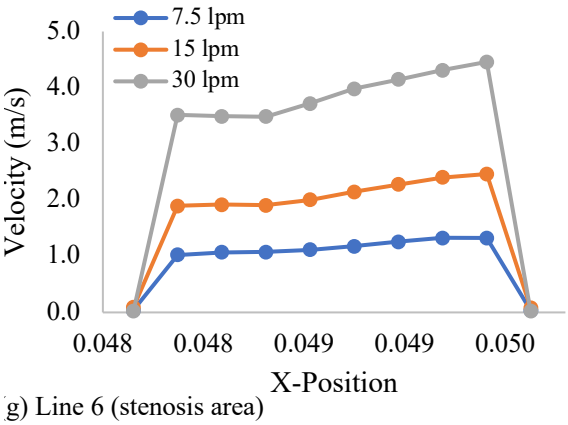

g) Line 6 (stenosis area)

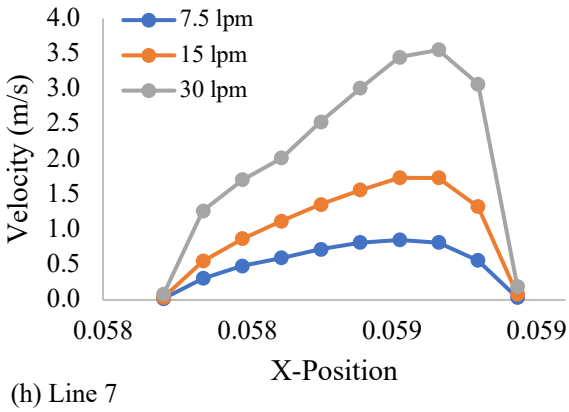

(h) Line 7

Figure 8.21 Selected line for velocity profiles of asymmetric lung model with right-stenosis area at 3rd generation: (a) Selected location (b) Line 1, (c) Line 2, (d) Line 3, (e) Line 4, (f) Line 5, (g) Line 6 at stenosis area, and (h) Line 7

In Figure 8.21, the velocities are continually increasing from the inlet and becoming lower again after through the stenosis region at 3rd generation (*Line 6*). The maximum velocity can be found in the stenosis area (*Line 6).*

- *Velocity Profiles for asymmetric lung model with right-stenosis area at4th generation*

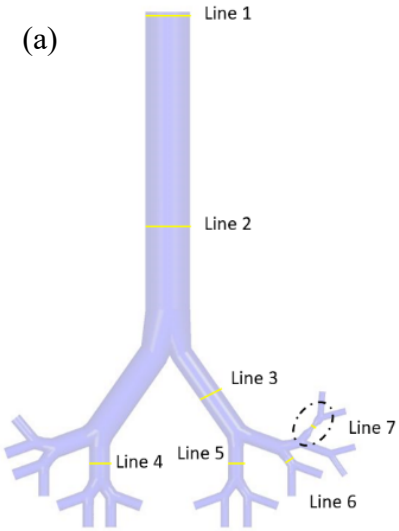

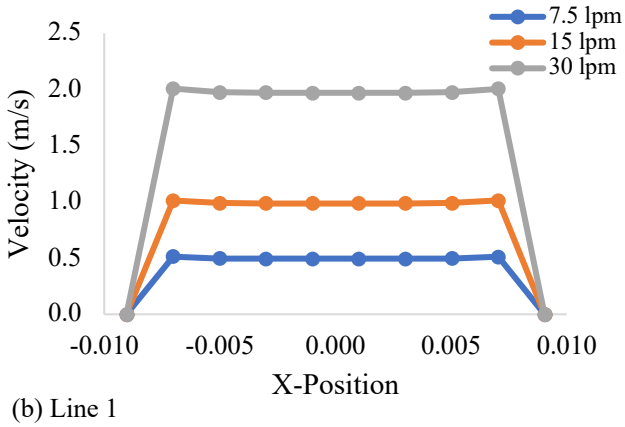

(b) Line 1

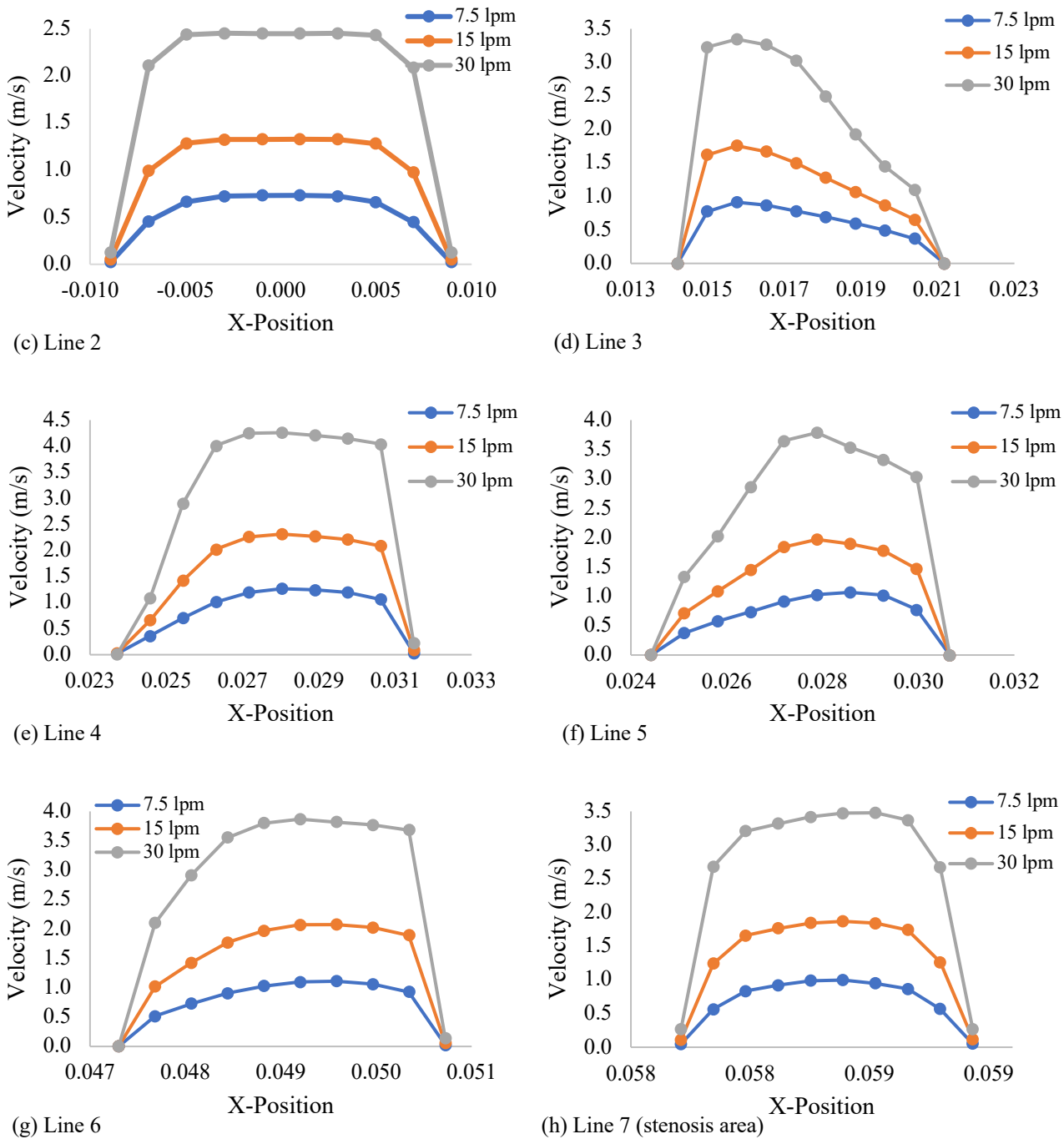

Figure 8.22 Selected line for velocity profiles of asymmetric lung model with right-stenosis area at 4th generation: (a) Selected location (b) Line 1, (c) Line 2, (d) Line 3, (e) Line 4, (f) Line 5, (g) Line 6, and (h) Line 7 at stenosis area

In Figure 8.22, the velocities are continually increasing from the inlet and becoming stable from the 2nd generation. The maximum velocity magnitude for this case is at the left-lung (*Line 4*).

The results of velocity profiles from five cases (Figure 8.18 to Figure 8.22) and from normal asymmetric lung case (Figure 8.4) could significantly indicate the relationship of the

stenosis region, the dimension of the airway, and velocity. The airflow velocity is repetitively increasing from the inlet for all flow rates. If compared to all cases, the velocity profiles at the inlet and the middle of the trachea have a similar velocity magnitude. The maximum velocity always occurs at the stenosis area, and after that, velocity continually decreases. A higher velocity always occurs at the left-lung, where it has a bigger diameter than the right-lung. In contrast, a lower velocity always initiates at the 4th generation if compared with the velocity at 1st to 3rd generations. Besides, the stenosis region at the 4th generation could have only a few effects to the velocity because it is lower than the velocity at the left-lung, which having a larger diameter. According to Islam et al. (2017b); Singh et al. (2020), higher airflow velocity at smaller airways or stenosis areas can be caused by airflow distribution within the lungs. With these conditions, air will flow to the opposite side because of the airflow resistance in these areas. To be concluded, the results in this report could support these authors because the maximum velocity for asymmetric lung without any narrow could be found at the left-lung (Figure 8.4d) where is larger than right-lung. If compared to other stenosis cases, the velocity at the left-lung (*Line 4*) will be lower than the velocity at stenosis areas.

Velocity Contours

Velocity contours represent fluid flow which discharges at the velocity point that is considered. It can be converted and represented as the average cross-sectional for the flow velocity at a selected point.

This report will provide two types of velocity contours with 30 lpm for the flow rates. The first type is velocity contour for the whole domain that will be generated at the XY plane. Another type is velocity contour at nine selected planes. Figure 8.23 shows the velocity contour at XY plane in different lung conditions. Figure 8.23a is for normal asymmetric lung, while Figure 8.23b is for asymmetric lung with stenosis area at generation 1. Figure 8.23c, d is the geometry for the stenosis area at 2nd generation of left and right lungs, respectively. Figure 8.23e, f is the representative at stenosis areas at 3rd and 4th generations.

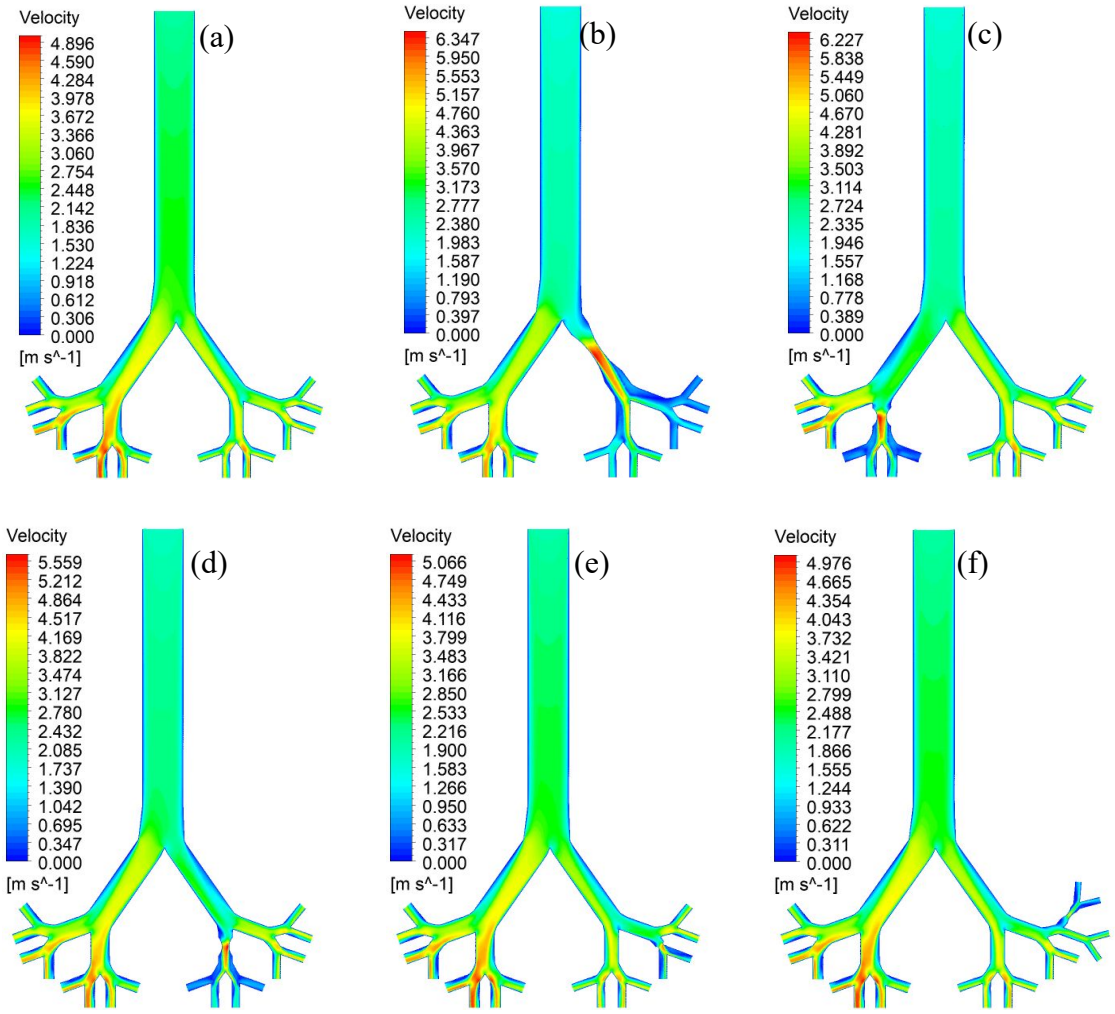

Figure 8.23 Velocity Contours at XY Plane for six lung models: (a) normal asymmetric lung, (b) stenosis-right at 1st generation, (c) stenosis-left at 2nd generation, (d) stenosis-right at 2nd generation, (e) stenosis-right at 3rd generation, and (f) stenosis-right at 4th generation.

The results from this section are similar to the results from the velocity profiles section. The airflow velocity is continuing to increase from the inlet for all cases. For normal asymmetric lung (Figure 8.23a), velocity is significantly increasing at the left-lung that has bigger airways, especially at the second branch. For the stenosis cases (Figure 8.23b, c, d, and e), maximum airflow velocity occurs at stenosis areas, but it is only for the cases that have stenosis areas at 1st and 3rd generation. For the stenosis area at 4th generation (Figure 8.23f), it does not have a considerable effect on airflow velocity. However, it can be seen that the bifurcation after the stenosis region has a lower airflow velocity if compared with normal asymmetric lung.

The randomly selected plans are generated at the various location from trachea (0 generation) to 4th generation by considering the comparison between the normal asymmetric lung and asymmetric lung with obstructive regions. Figure 8.24 shows the location of selected

planes from six different cases. Figure 8.24a is for an asymmetrical case without any narrow. Figure 8.24b is for the case that has narrow at 1st generation, while Figure 8.24c, d is for the cases that have narrows at 2nd generation in the left and right lungs. Figure 8.24e, f is for the models that have narrows at 3rd and 4th generations. Figure 8.24 is the representative of the comparison of velocity contour between six different lung airways.

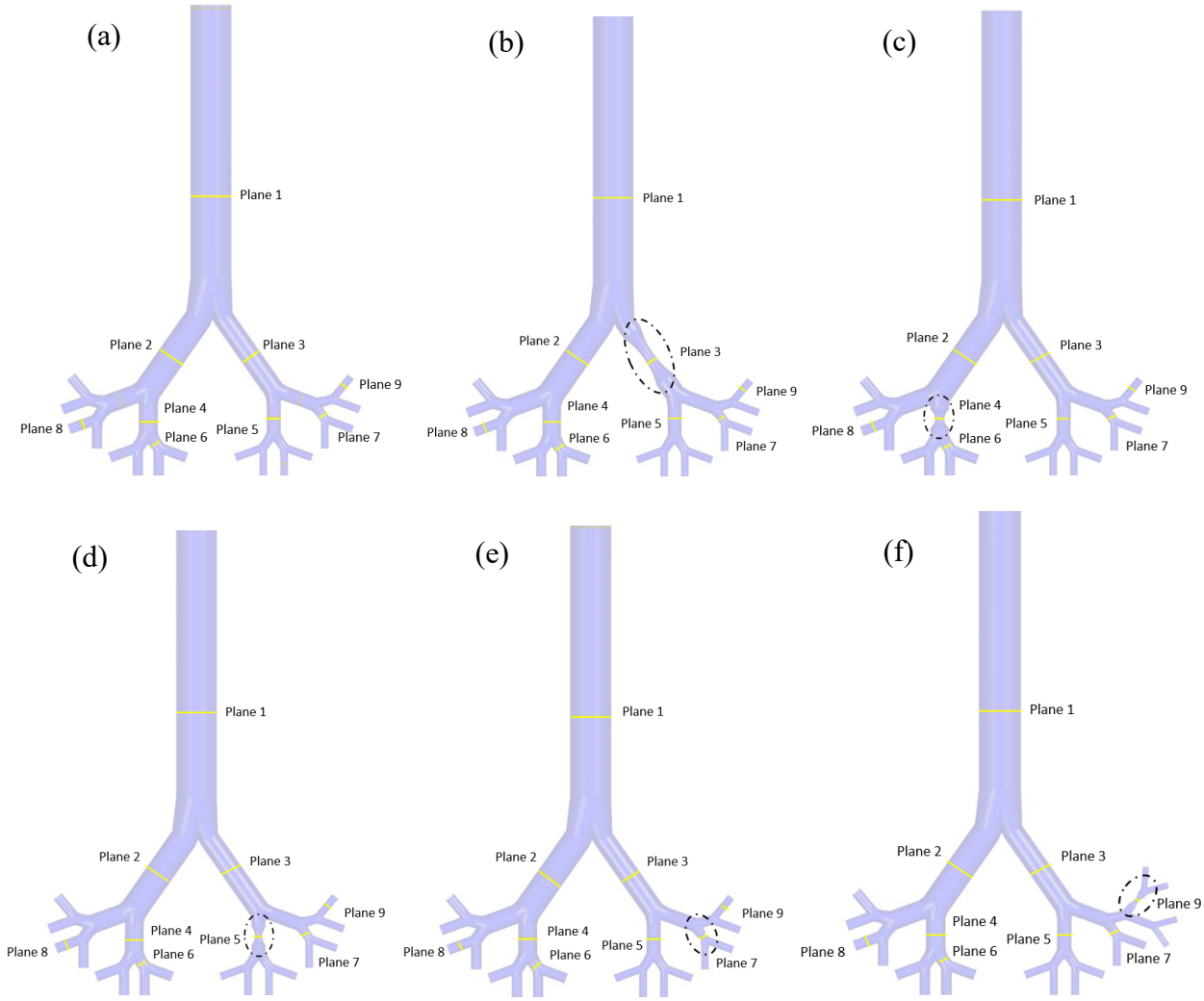

Figure 8.24 Selected planes for different positions of asymmetric lung model and asymmetric lung model with stenosis areas: (a) normal asymmetric lung, (b) stenosis-right at 1st generation, (c) stenosis-left at 2nd generation, (d) stenosis-right at 2nd generation, (e) stenosis-right at 3rd generation, and (f) stenosis-right at 4th generation.

Figure 8.25 indicates that the airflow velocity in the middle of the trachea (*Plane 1*) for all cases has a similar pattern. For the 1stgeneration (*Planes 2* and *3*), the flow patterns are still similar except for the flow pattern at the stenosis region (Figure 8.25b). Similarly, the flow patterns at the 2ndgeneration (*Planes 4* and *5*) are also similar except at stenosis areas (Figure 8.25c, d) that are located in different lung sides. Moreover, the area, that is under the stenosis

area, also has a different flow pattern (Figure 8.25b of *Plane 5*). *Plane 6* and *7*are generated to see the airflow patterns at 3rd generation. It can be seen that the airflow pattern in the stenosis area (Figure 8.25e of *Plane 7*) does not differ from other areas. However, it is obvious that the areas that connect to the stenosis area have different airflow patterns. For deep details of changed airflow patterns, *Plane 6* of Figure 8.25c and *Plane 7* of Figure 8.25b vary from others because of the connection between stenosis areas for generation 1 and 2 respectively. In terms of the airflow pattern at 4th generation (*Planes 8* and*9*), it is also similar to 3rd generations that stenosis area does not make a change in airflow patterns (*Plane 9* of Figure 8.25f for stenosis area at 4th generation). Furthermore, only *Plane 9* of Figure 8.25b has a different pattern because of directly connecting to the stenosis area from 1stgeneration.

Overall, it can be summarized that the airflow pattern can change due to the obstructive areas. And then, other flow patterns, which are under obstructive airways, usually have different airflow patterns if compared with other cases without obstruction. Based on the study from Singh et al. (2020), the airflow velocity is significantly affected by several factors such as turbulence fluctuation at narrow section, the shape of airways in different conditions and the force that is from pressure driven. However, obstructions at 3rd and 4th generations could not have significant effects on airflow patterns.

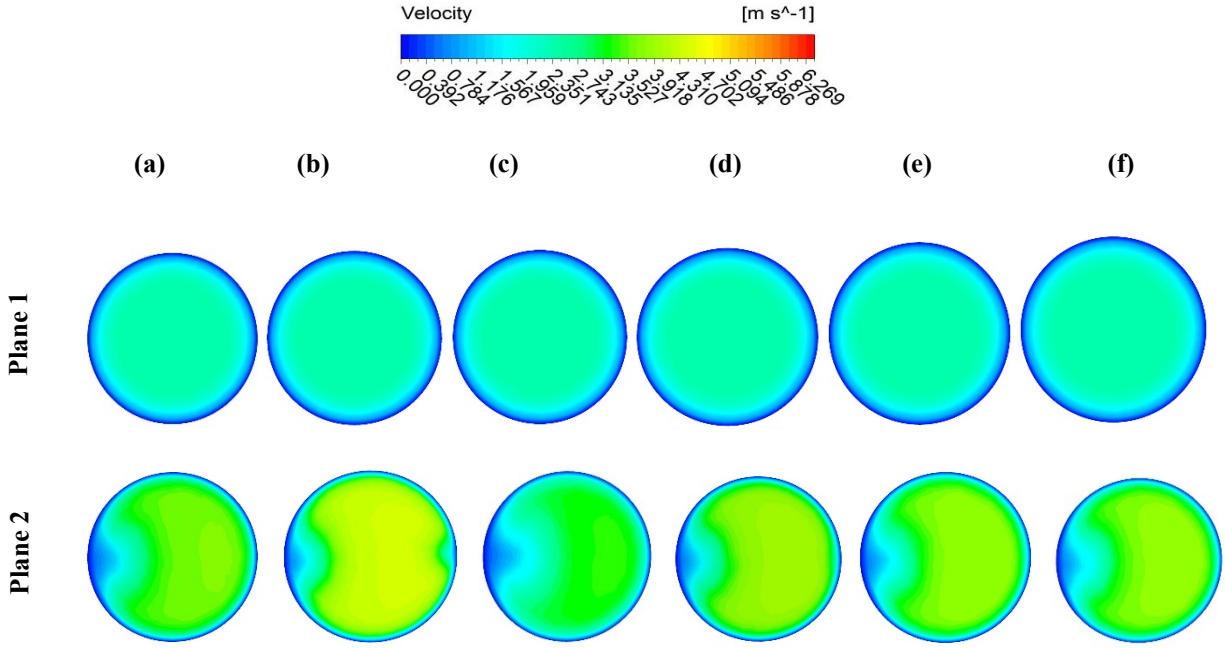

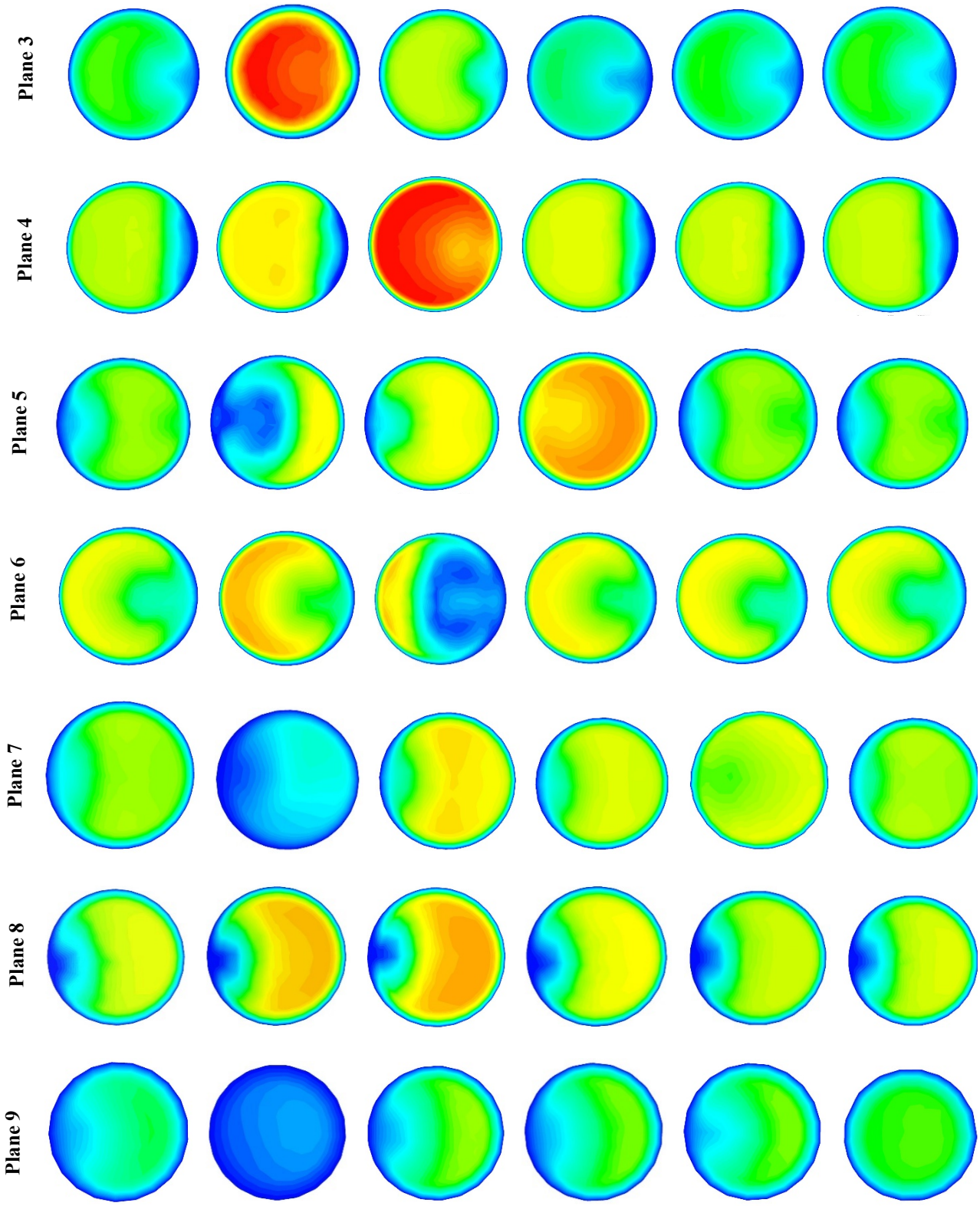

Figure 8.25 Velocity contours at different positions of asymmetric and stenosis airways at 30 lpm: (a) normal asymmetric lung, (b) stenosis-right at 1st generation, (c) stenosis-left at 2nd generation, (d) stenosis-right at 2nd generation, (e) stenosis-right at 3rd generation, and (f) stenosis-right at 4th generation.

8.5.2.2 Pressure Drop

Pressure drop is significantly related to the airways resistance. Airways resistance is defined as the thing that resists flowing, which is caused by the friction forces. By the degree of the resistance to flow within the airways usually depends on the flow characteristics that are laminar or turbulent, the viscosity of the gas, and the dimensions of the airways (Esther et al. 1973). This section contains two main parts that are related to airway pressure. The first one is the pressure drop, and the second one is pressure contours.

Pressure Drop

The randomly selected planes are generated from the middle of the trachea to 4thgeneration for various asymmetric lung models. The pressure drop is calculated based on 10 µm for the particle size. Three different flow rates are considered in this part in order to evaluate the changes in pressure drop. Figure 8.26 represents the pressure drop at different selected planes for all six cases by Figure 8.26a is for flow rate at 7.5 lpm, Figure 8.26b is for 15 lpm, and Figure 8.26c is for 30 lpm.

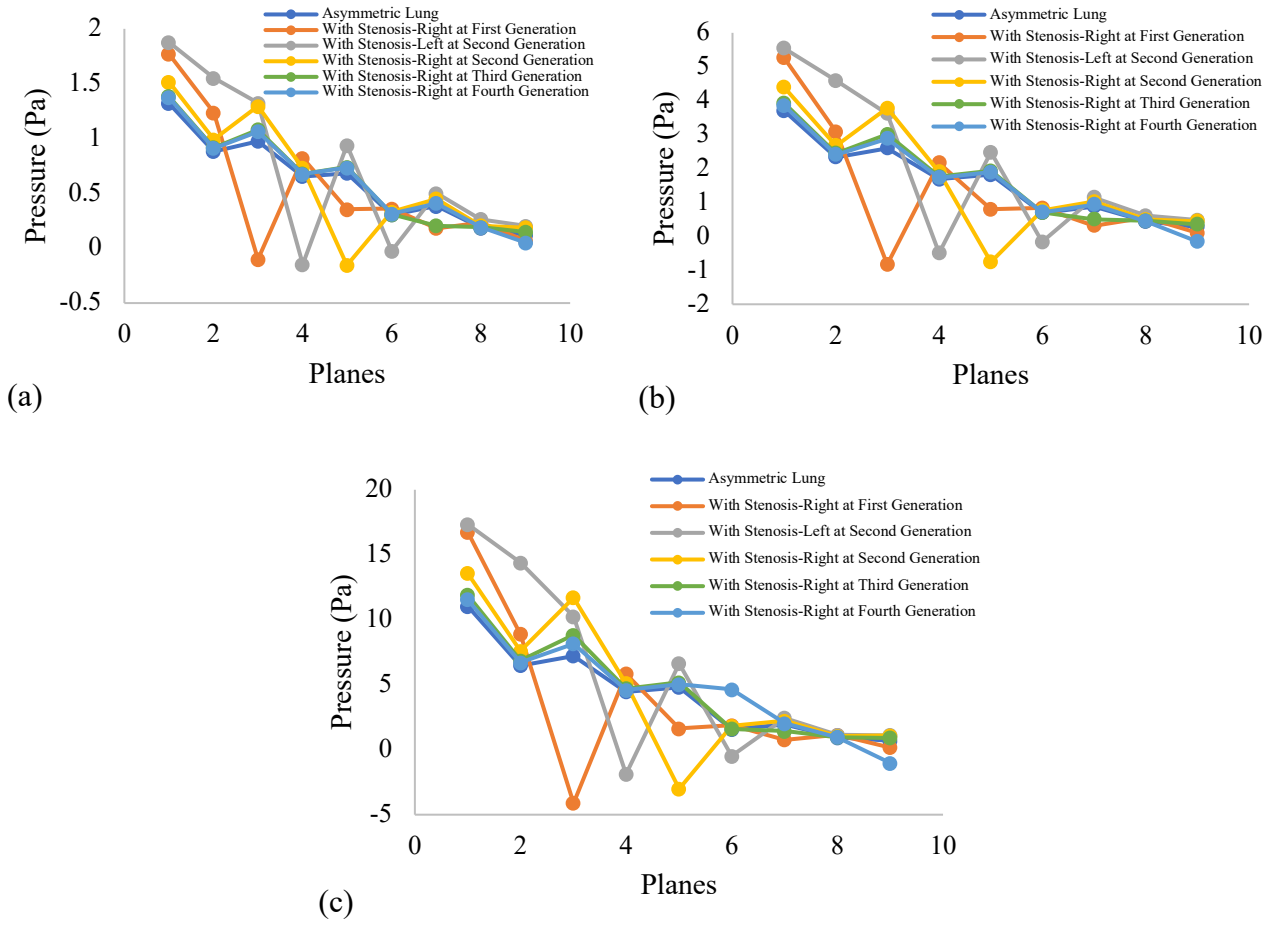

Figure 8.26 Pressure drop at different plane positions for asymmetric lung and asymmetric lung with stenosis airways: (a) 7.5 lpm, (b) 15 lpm, and (c) 30 lpm.

According to Singh et al. (2020), atmospheric pressure must be higher than the airway pressure because of the direction of the air, which always flows from the higher pressure zone to the lower pressure zone. From the results of Figure 8.26, it is obvious that other selected planes from all six cases with three different flow rates have a lower pressure than the initial pressure on *Plane 1*. Moreover, the highest pressure drop always occurs in an area that has an obstruction. For the lowest flow rate at 7.5 lpm (Figure 8.26a), the maximum pressure drop is located in the stenosis area at the right-lung of generation 2 (*Plane 5*). However, both flow rates at 15 lpm and 30 lpm (Figure 8.26b, c) have the highest pressure drop at the stenosis area of the right-lung at generation 1 (*Plane 3*). In contrast, the highest pressure is also located at *Plane 1* of stenosis-left at the 2nd generation, which has 30 lpm for the flow rate (Figure 8.26c). For normal asymmetric lung without having any stenosis section, initial pressure in this case is lower than other cases that consist of stenosis areas. More details for stenosis cases, it can be seen that after throughout stenosis area, under branch, which directly connects to the stenosis branch, still has a higher pressure drop.

To summarize, it can be noticed that the flow rate can influence the level of pressure drop. If compared to all three flow rates, the highest pressure drop at the stenosis area is located at the highest flow rate that is 30 lpm. In addition, stenosis condition also has an essential effect on pressure drop. Referred to Singh et al. (2020), airway pressure could influence human breathing. A higher pressure drop in the stenosis region could increase airway resistance. As a result, it causes difficulty in inhaled conditions.

Pressure Contours

Pressure contours present the pressure variation within the domain. It could be changed based on the fluid flows during the domain. XY Plane is created at the center of all six cases with 30 lpm of flow rate and 10 μm for particle size. Figure 8.27 is representative of pressure contours at XY Plane for different lung conditions. Figure 8.27a is for an asymmetrical lung model, whereas Figure 8.27b involves the stenosis area at 1st generation. Figure 8.27c, d is for left and right stenosis cases at 2nd generation. Figure 8.27e, f is for stenosis conditions at 3rd and 4th generations, respectively.

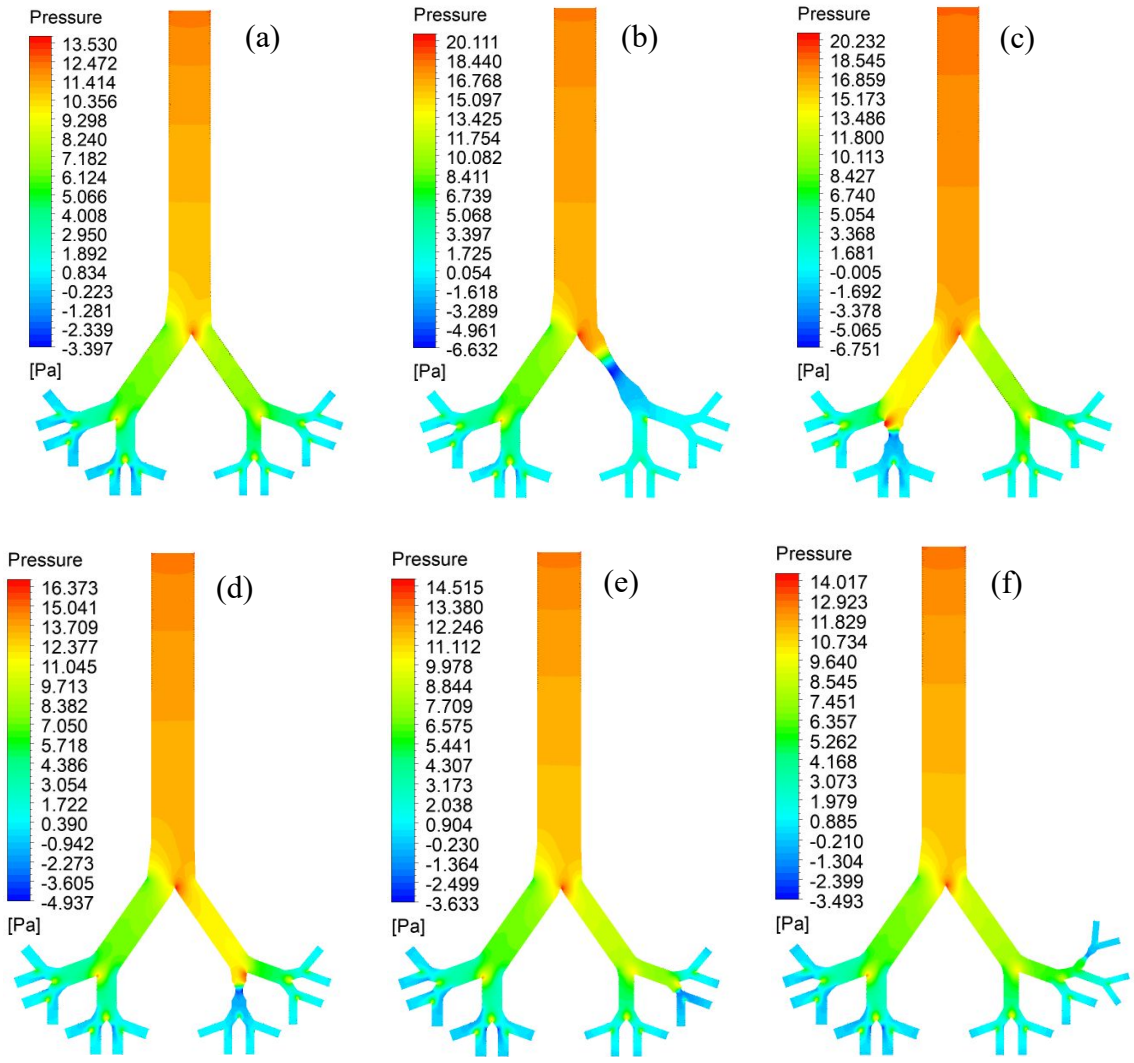

Figure 8.27 Pressure Contours at XY Plane for six lung models: (a) normal asymmetric lung, (b) stenosis-right at 1st generation, (c) stenosis-left at 2nd generation, (d) stenosis-right at 2nd generation, (e) stenosis-right at 3rd generation, and (f) stenosis-right at 4th generation.

To compare all six cases, the highest pressure is found at the first bifurcation, and then the pressure continually decreases along the airways. However, the pressure becomes an increase again in the region, where it is nearly the bifurcation and has a significant increase in the area before the obstruction. In contrast, the areas before stenosis regions at 3rd and 4th generations do not have any higher pressure due to the length and dimension of the airways. Moreover, the lowest pressure is usually found at the center of the obstructive area. After that, it is increasing again. For asymmetric lung without stenosis condition (Figure 8.27a), the overall pressure in this case is similar to other cases except for the branches that are related to the stenosis regions.

Consequently, there are higher pressure at a bifurcation and the nearly obstructive region. The lowest pressure is always found at the center of the obstructive region. Based on

the study of Nowak et al. (2002), pressure in bifurcating airways will be different based on the airway resistance, which is caused by the lung volume as the dimension of the airway and overall flow rate. The pressure in all six cases can vary because of various dimensions. The overall pressure at right-lung is higher than left-lung because of smaller dimension.

8.5.2.3 Wall Shear

Shear stress is classified as one of six types of stresses. However, wall shear stress is normally known as the shear stress of fluid which is always occurring in the layer next to the wall of a domain. It has been considered for the clinical field because of the fluid characteristic. In normally, fluid has a fastest-flowing at the center of the domain and slowest flowing close to the wall. Moreover, wall shear stress can be generated based on the flow friction that is related to velocity magnitude.

In this section, all six lung airway models are simulated with 30 lpm for flow rate and 10 μm for the particle size. Figure 8.28 is the representative of the wall shear contour for six different cases. Figure 8.28a is for normal asymmetric lung airway, whereas Figure 8.28b is for asymmetric lung with stenosis area at 1st generation. Figure 8.28c, d is for the lung with stenosis areas at the left and right lungs at 2nd generation. Figure 8.28e, f is for the lung with stenosis areas at 3rd and 4th generation, respectively.

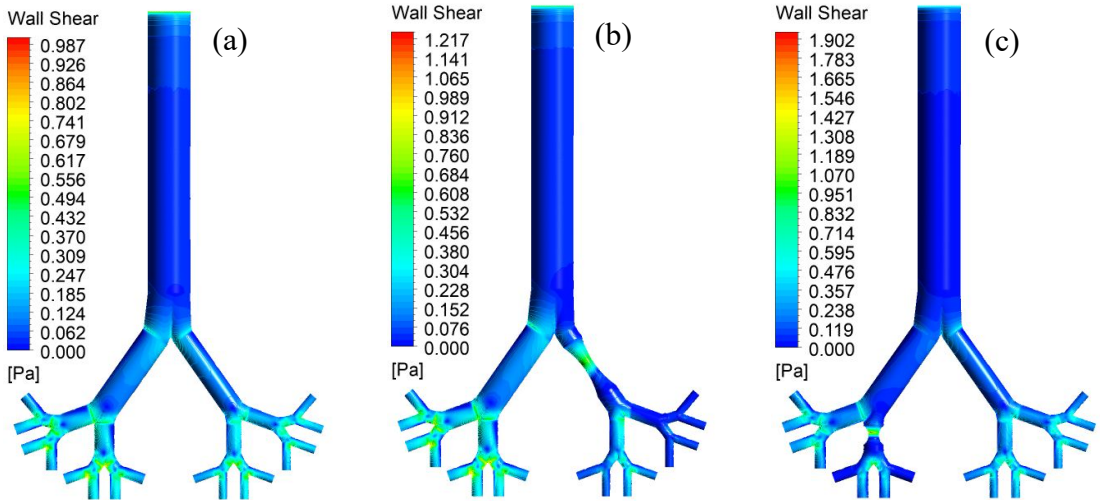

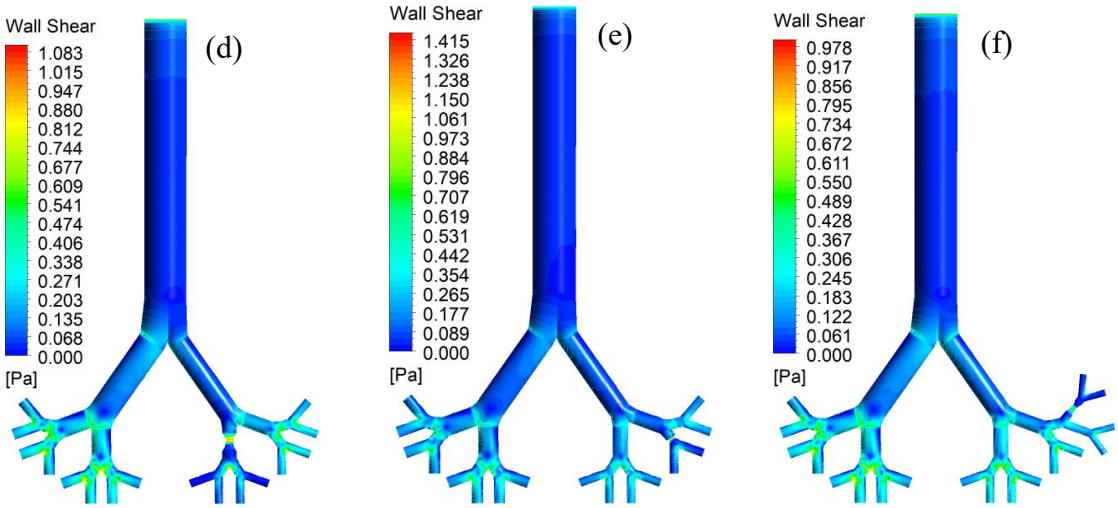

Figure 8.28 Wall shear for six lung models at 30 lpm: (a) normal asymmetric lung, (b) stenosis-right at 1st generation, (c) stenosis-left at 2nd generation, (d) stenosis-right at 2nd generation, (e) stenosis-right at 3rd generation, and (f) stenosis-right at 4th generation.

From these figures, wall shear stress is higher at the initial airway, becomes more stable, and starts to be higher again at the first bifurcation area. It can be seen that most of the bifurcations have a higher wall shear stress excepting the branch, which directly connects to the stenosis area. In terms of the stenosis area, it can be found that the stenosis area has an essential effect on wall shear stress. Most stenosis areas have a higher wall shear stress in the middle of itself, and lower branches will have a lower wall shear stress.

The results in this report are similar to the study of Cebral & Summers (2004). The pressure and shear stress are always opposite to each other. From the previous discussion on pressure contours, the pressure is found lower in the stenosis area, whereas shear stress is higher in this area. Furthermore, wall shear stress at the left lung has a higher magnitude if compared with the right lung. In a nutshell, airway dimension and bifurcation can influence to the wall shear stress.

8.5.2.4 Turbulence Intensity

Turbulence intensity is representative of the level of turbulence, which uses for the intensity measurement of the flow fluctuations. The level of the turbulence intensity is generated by the contour of the whole domain. The flow rate at 30 lpm and particle size at 10 µm are used to be an input data for all lung models. Figure 8.29 shows the turbulence intensity contour for six different airway conditions. Figure 8.29a is asymmetric airway without any narrow, whereas Figure 8.29b and others are the airways with stenosis areas at different generations, which are

from 1st to 4th generations.

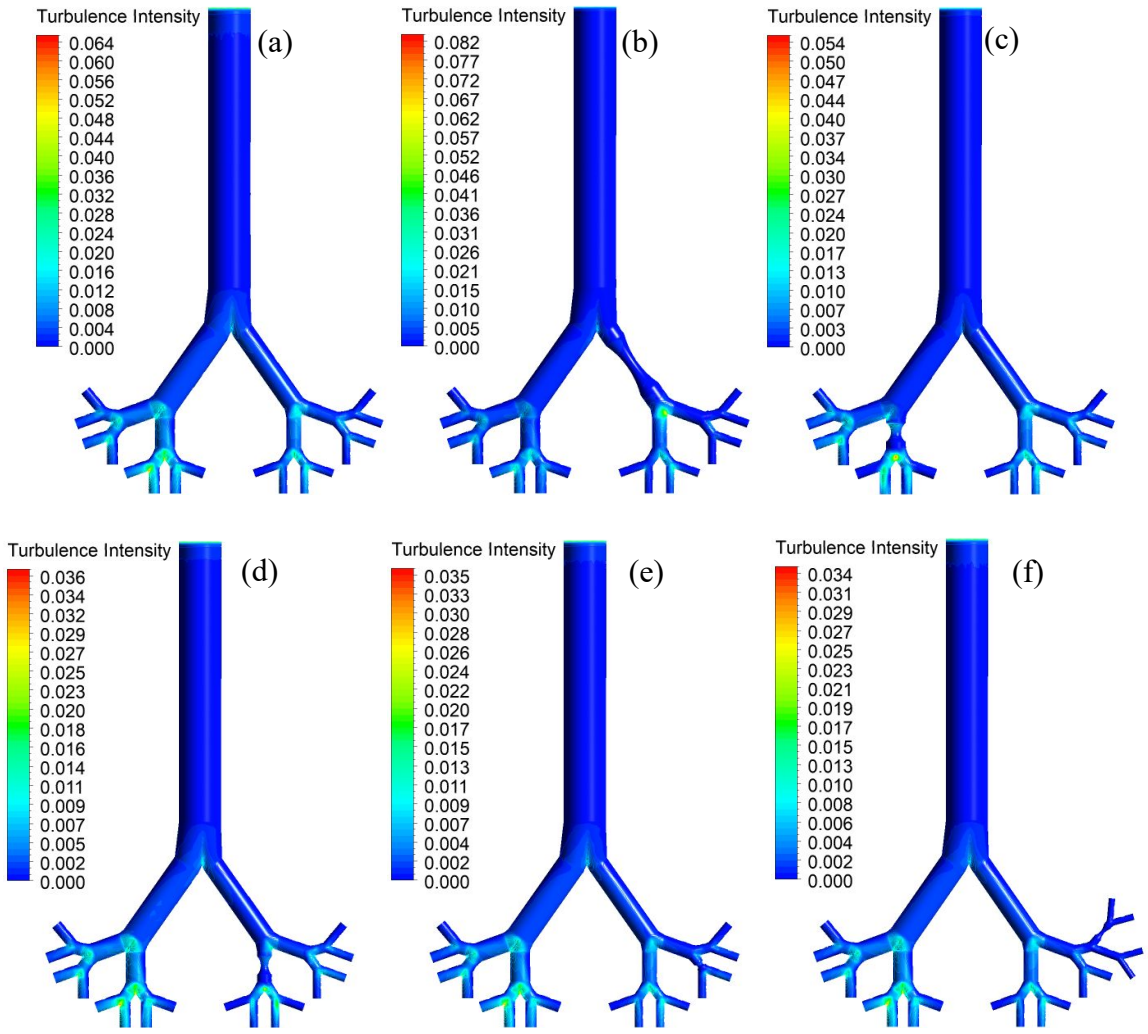

Figure 8.29 Turbulence intensity contour for six lung models at 30 lpm: (a) normal asymmetric lung, (b) stenosis-right at 1st generation, (c) stenosis-left at 2nd generation, (d) stenosis-right at 2nd generation, (e) stenosis-right at 3rd generation, and (f) stenosis-right at 4th generation.

From Figure 8.29, turbulence intensity often occurs in the inlet region and most of the bifurcations. It can be seen that the level of turbulence intensity from normal asymmetric lung (Figure 8.29a) is quite different from other lungs that have stenosis areas (Figure 8.29b to Figure 8.29f). The lobes, which are under stenosis airway, obviously have a higher turbulence intensity if compared to the normal case (Figure 8.29a). From Figure 8.29b and Figure 8.29c, the lung, which is opposite stenosis-lung, also has lower turbulence intensity if compared to normal airways (Figure 8.29a). However, stenosis areas at 3rd and 4thgenerations (Figure 8.29e, f) can have few effects on the turbulence flow. Referred to Ma & Lutchen (2009), the authors claimed that only from the upper airway that can generate turbulent flow. In contrast, the result

from this chapter and Singh et al. (2020) have similar points that stenosis area could influence the flow pattern, which can increase turbulence intensity.

There are nine selected planes that are created to calculate the turbulence intensity values in order to make the comparisons between six models. By this calculation is based on the flow rate at 30 lpm. Figure 8.30 shows the turbulence intensity values at randomly selected plans with different airway conditions.

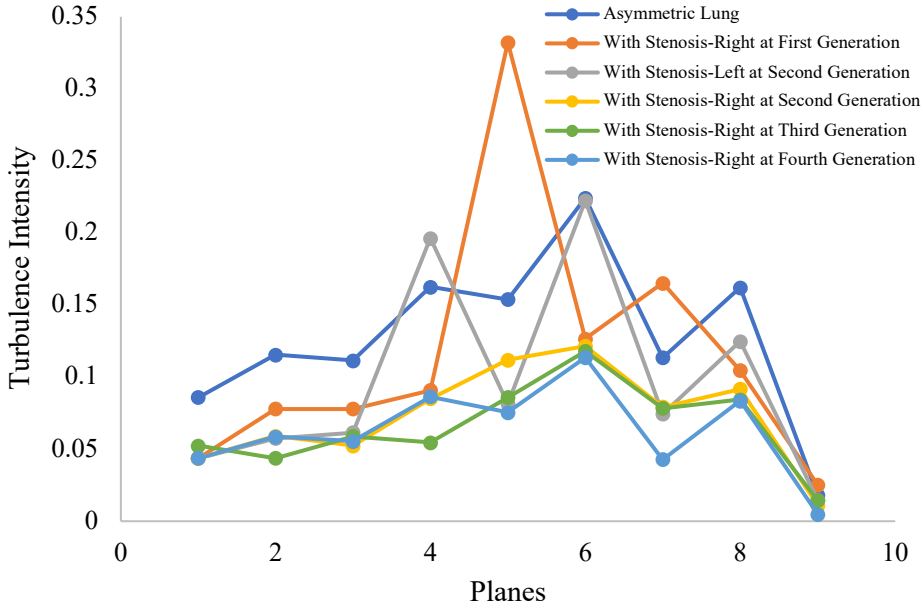

Figure 8.30 Turbulence intensity at different plane positions for six lung models at 30 lpm

From the above figure, the airway with the stenosis area at 1st generation case has the highest turbulence fluctuation at *Plane 5*, which is under of the stenosis branch. The secondary highest turbulence values are found from two cases at *Pane 6* which are the cases that have stenosis area at left lung at 2nd generation and the case that have no stenosis area. However, all six cases have similar lowest turbulence values at *Plane 9* where it locates in 4th generation. It can be summarized that having a stenosis area can increase the turbulence fluctuation, especially at 1st generation. On the other hand, having a stenosis area at 4th generation could have an insignificant effect on turbulence values.

To conclude, overall turbulence intensity from both contours and plotting graph, turbulence intensity can be influenced by the stenosis area but only for 1st generation and 2nd generation. Stenosis areas at 3rd and 4th generations could have a minor effect on flow patterns and turbulence intensity.

8.5.2.5 Particle Transport

Particle transport in lung airways plays a vital role in drug delivery. At the same time, it can also induce respiratory diseases because of inhaled harmful substances such as dust and gaseous pollutants. There are various types of these substances in the environment that are classified based on shapes and sizes ranging from smaller sizes to larger sizes (Asgharian et al. 2014; Farghadan et al. 2019).

In order to enhance the understanding of the particle transport within asymmetric lung airways with stenosis area at different generations of the lung, this report will investigate and analyze the particle deposition under various conditions. Then, this report will provide a comparison based on two variables from deposition efficiency and deposition fraction.

Deposition Efficiency

Deposition efficiency is known as the ratio of the number of particles that having various sizes and the amount of each particle size that is deposited at a given area. The particle deposition efficiency for six lung conditions is calculated based on three different flow rates and provided as Figure 8.31.

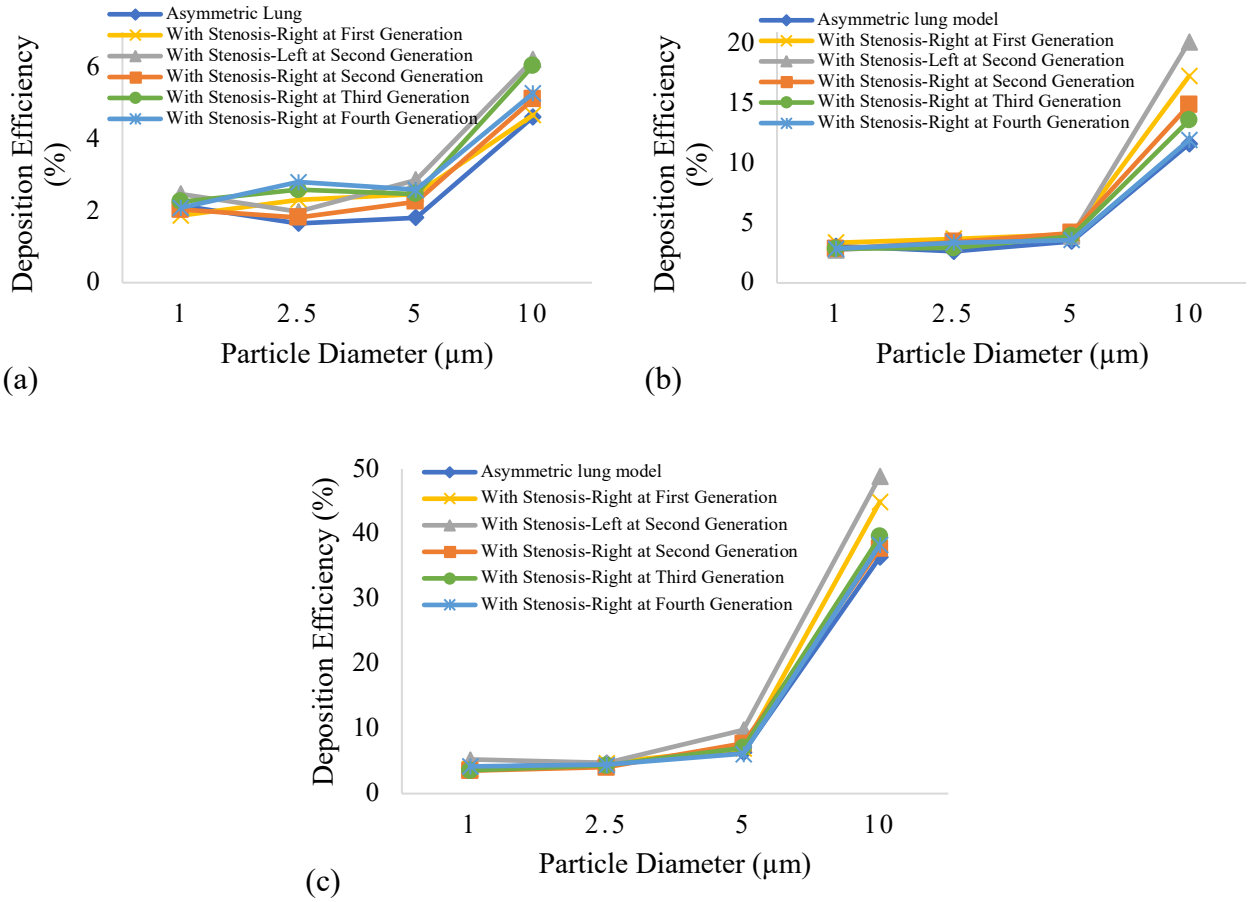

Figure 8.31 Deposition Efficiency in different region of asymmetric lung and asymmetric lung with stenosis areas: (a) 7.5 lpm, (b) 15 lpm, and (c) 30 lpm.

Obstruction has an extreme effect on deposition efficiency. From the three flow rates (Figure 8.31), it is obvious that the stenosis area at 2nd generation has the highest deposition efficiency. Moreover, the stenosis area at 1st generation has second-highest deposition efficiency if compared to the asymmetric lung without any stenosis area. Another important thing is that the flow rate could influence the deposition efficiency. Flow rate at 30 lpm (Figure 8.31c), could cause the highest deposition or trapped as 49% in the case of 10 µm for particle size. In contrast, other flow rates at 7.5 lpm and 15 lpm have deposition rates as 6% and 20%, respectively.

At higher flow rate, especially with larger particle size, can increase the deposition efficiency rate because of having greater particle inertia (van Ertbruggen et al. 2004; Ma &Lutchen 2009; Singh et al. 2020). It can be concluded that the flow rate and particle size could influence deposition efficiency. However, based on the above discussion, the stenosis area could increase greater deposition efficiency, especially the stenosis area at 1st and 2nd generations.

Deposition Fraction

Deposition fraction is referred as the number of particles that focusing only one size and the amount of that particle size deposited at a given area. Figure 8.32 shows the deposition fraction of different-diameter particles in six different cases.

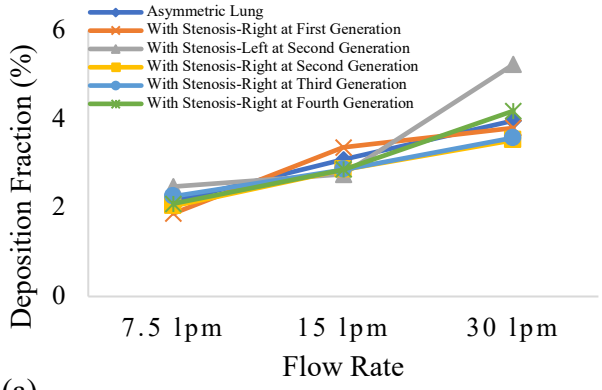

(a)

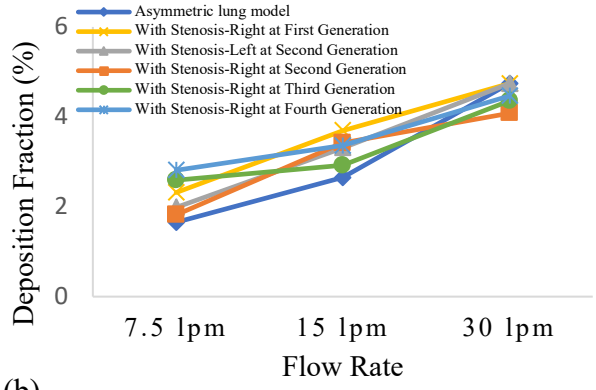

(b)

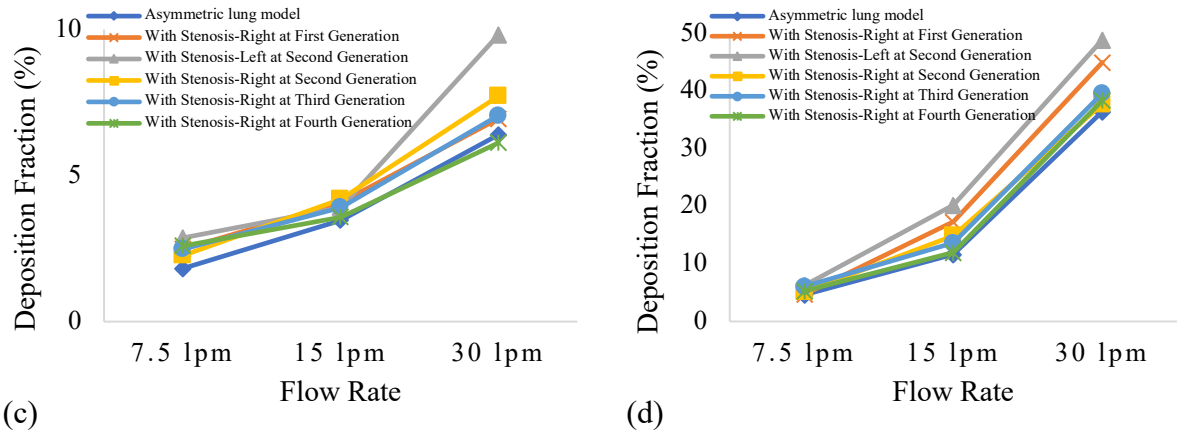

Figure 8.32 Deposition Fraction of different-diameter particles in asymmetric lung and asymmetric lung with stenosis airways: (a) 1 µm diameter, (b) 2.5 µm diameter, and (c) 5 µm diameter, and (d) 10 µm diameter

From Figure 8.32, it can be seen that the particle sizes as 1 µm and 2.5 µm (Figure 8.32a, b) have a similar deposition fraction approximately 5% at 30 lpm, while the flow rate at 7.5 lpm has deposition fraction around 2%. In case of particle size as 5 µm (Figure 8.32c), stenosis case at second generation has a higher deposition fraction around 10% if compared to other stenosis cases which have deposition fraction around 4% to 7%. In terms of the particle size as 10 µm (Figure 32d), a higher deposition fraction is around 49% at 30 lpm of the flow rate. This case is still the case of the stenosis area in the second generation. Furthermore, it is also the highest value if compared to other conditions.

In conclusion, the number of particle deposition of deposition fraction is usually based on the particle diameter, flow rate, and density (Islam et al. 2015; Lalas et al. 2017; Singh et al. 2020). For example, greater particle diameter will have a higher particle deposition rate. In the same way, a higher flow rate will have a higher particle deposition rate. In terms of obstructive cases, the smaller airway volume can increase the number of particle deposition (Singh et al. 2020). From this chapter, obstructive areas in the first and second generations have a particular effect on increasing the deposition fraction rate.

The various particle sizes have been used to be an inlet injection into all six lungs under stenosis conditions in different areas with 30 lpm of flow rate. Figure 8.33 shows the particle deposition scenario with different six lung conditions.

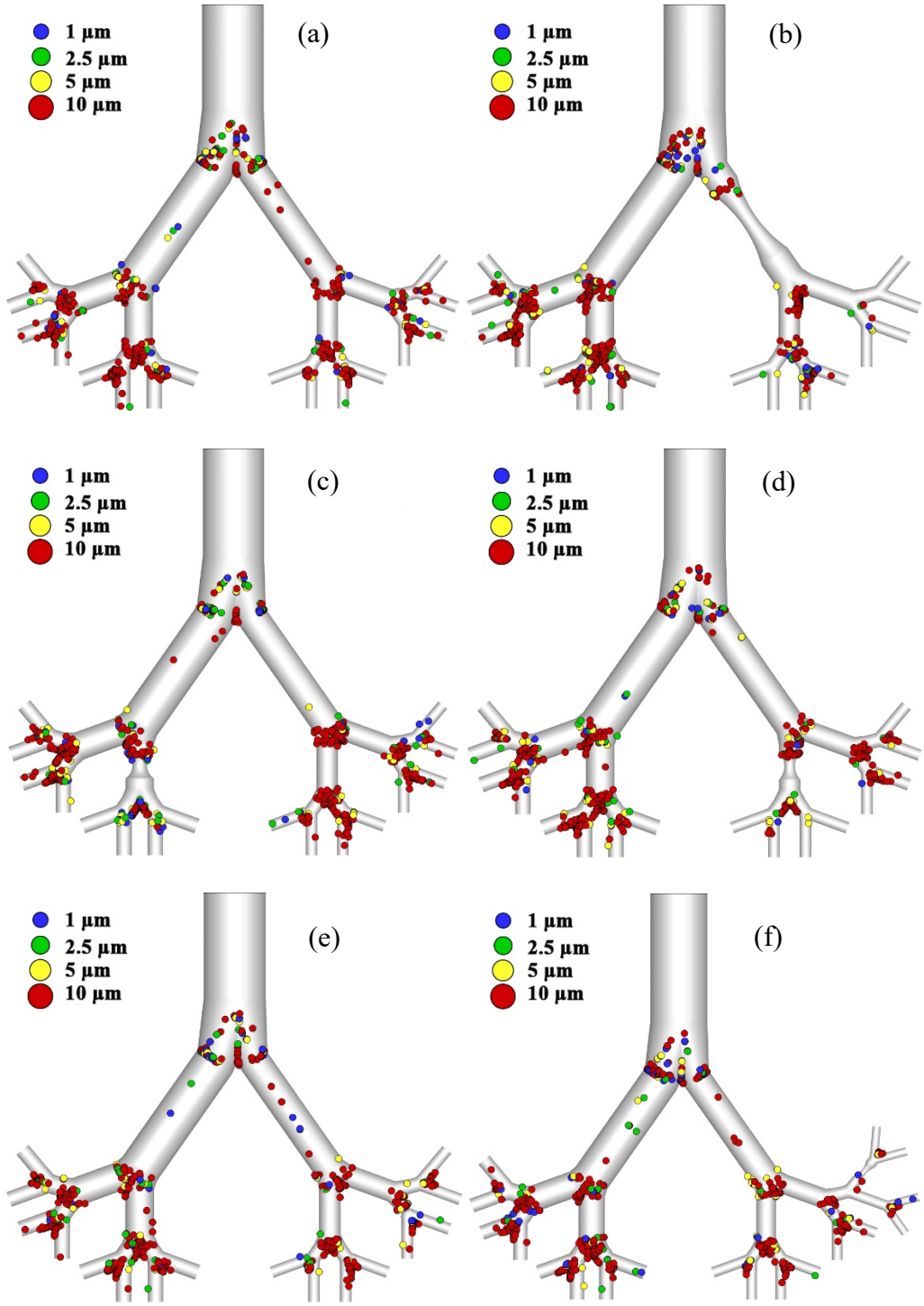

Figure 8.33 Particle deposition scenario at 30 lpm for six lung models: (a) normal asymmetric lung, (b) stenosis-right at 1st generation, (c) stenosis-left at 2nd generation, (d) stenosis-right at 2nd generation, (e) stenosis-right at 3rd generation, and (f) stenosis-right at 4th generation.

Overall, in six cases, the majority of particles are trapped at the airway, which is opposite the stenosis area, especially for the largest particle size as 10 µm. All of these particles are trapped at the wall of bifurcation for each generation. The lobe of second-generation has more particle deposition if compared to other areas. In cases of asymmetric lung model without stenosis area

(Figure 8.33a), the left lung has higher particle deposition than the right lung because of having a larger diameter.

To summarize, the majority of particles are usually trapped at the wall of a bifurcation (Balashazy & Hoffman 1995; Farghadan et al. 2019). The results of this ~~report~~ study can support this idea. An increase in velocity at the stenosis area could influence the particle pattern, which is significantly deposited at the bifurcation area (Singh et al. 2020). In addition, it can be summarized that the largest particle size at 10 μm is usually trapped in the bifurcation of second generation.

8.6 Limitation of the Study

This chapter has used zero-gauge pressure as the outlet boundary for all lung airway models. but in real life, some unknown pressures should be inside the lung in the third and fourth generations. In terms of wall condition, it has been considered as stationary wall condition which has no dynamic wall motion. Moreover, this report only considers the inhaled breathing for both airflow and particle transport. This report focuses on the abnormal lung having asymmetric condition with stenosis area, not considering for airway inflammation cases.

8.7 Conclusions

In this chapter, the airflow and particle transport has been investigated under an asymmetric lung airways condition. A normal asymmetric lung has been compared to another two asymmetric lungs with having aging effects that result in having smaller diameters. Moreover, this study also compares a normal asymmetric lung to other asymmetric lungs with stenosis sections in the different generations beginning from the first generation to the fourth generation. Calculations have been performed based on two variables that are flow rates and particle sizes. The following information will be the conclusion for the overall of this study:

- *The airflow velocity*

For effects of aging cases: The airflow velocity magnitude is influenced by the volume in the lung airways. A smaller diameter could generate higher velocity magnitude especially for the left-lung airways

For stenosis cases: The airflow velocity could be influenced by the stenosis section. The velocity in this area is higher than in other areas if compared to the normal asymmetric lung. However, it seems that the airflow velocity can be increased by stenosis conditions at first generation to the second generation, while the stenosis areas at third and fourth generations could not have much effect on velocity magnitude.

- *Pressure*

For effects of aging cases: The airway volume and the flow rate can affect to pressure levels. A smaller airway could lead pressure to be a higher level. Among the three cases, the maximum pressure is located at the trachea for all cases while the minimum pressure has been found at the fourth generation.

For stenosis cases: The level of the pressure is depended on the airway volume and the flow rate. The overall pressure at right-lung is higher than left-lung because of having a smaller dimension. The maximum pressure has been found in the trachea region, while the lowest pressure has located at the stenosis area where it is at the right-lung of the first generation.

- *Wall shear*

For effects of aging cases: The bifurcation can have a greater effect on wall shear stress, whereas the volume of the lung airways can have a minor effect on shear stress at the wall.

For stenosis cases: Airway dimension and bifurcation can have a significant effect on the wall shear stress. Wall shear is found to be higher at the bifurcation and in the middle of the stenosis area.

- *Turbulence intensity*

For effects of aging cases: Normal asymmetric lung can generate more turbulence intensity while smaller airways have a lower turbulence intensity and also have similar levels. The airflow begins to be stable from the fourth generation of the airways, and it tends to be continually stable for all lower generations.

For stenosis cases: Overall turbulence intensity of the whole lung is similar for all six cases. Local turbulence intensity has been found to be higher at the bifurcation and the stenosis area where it is only for first and second generations. On the other hand, stenosis areas at the third and fourth generations could not have a significant effect on turbulence intensity.

- *Particle deposition*

For effects of aging cases: Both deposition efficiency and deposition fraction are based on the particle size, flow rate, and airway volume. A smaller diameter of a 20% reduction usually has higher deposition efficiency and deposition fraction in different flow rates and particle sizes. The bifurcation for all generations can deposit more particles, especially for 10 μm size.

For stenosis cases: The trend of deposition efficiency and deposition fraction is based on the stenosis area, particle size, and flow rate. The deposition efficiency and deposition fraction for stenosis areas at first and second generations tend to be higher than the stenosis area at other generations. The particles are usually trapped at the wall of a bifurcation for each generation. The majority of particle size as 10 μm is deposited in the bifurcation of second-

generation.

This study has presented the numerical simulation of the airflow and particle transport in asymmetric human lungs with stenosis and the effects of aging conditions. Eight different lung models have been used to analyze the velocity profiles, pressure drop, wall shear stress, turbulence intensity, and particle deposition. The model has been developed based on symmetric lung from Weibel's model by reducing the diameter 25% for the whole right-lung and 50% for stenosis areas. In terms of the effects of aging cases, the diameter for the whole model of the asymmetric lung has been reduced by 10% and 20% sizes and remaining the same lengths for the whole model. This study enhances the understanding of the effects of the obstruction and the aging on the airflow patterns and particle movements within abnormal human lungs. The understanding of pressure analysis could be useful for clinical treatment, especially with the severe cases coming with the usage of mechanical ventilation. The knowledge of particle transport could improve the understanding of the drug-aerosol delivery passing stenosis regions. Respiratory diseases, such as asthma and COPD may have variant stenosis conditions as well as the effect of aging on the respiratory system. The comprehensive study of the asymmetric lung with stenosis areas and the aging's effects should be examined in more variables. In a further study, specific lung disease should be considered.

References

Ahmed, S.M. & Athar, M. 2015, Mechanical ventilation in patients with chronic obstructive pulmonary disease and bronchial asthma. *Indian journal of anaesthesia* 59, no. 9: 589-598.

Asgharian, B., Price, O.T., Oldham, M., et al. 2014.Computational modeling of nanoscale and microscale particle deposition, retention and dosimetry in the mouse respiratory tract. *Journal of Inhalation Toxicology* 26, no. 14: 829-842.

Augusto, L.L.X., Lopes, G.C. & Goncalves, J.A.S. 2015.A CFD study of deposition of pharmaceutical aerosols under different respiratory conditions. *Brazilian Journal of Chemical Engineering* 33, no. 3: 549-558.

Australian Institute of Health and Welfare 2019. *Asthma*. Cat. no. ACM 33. Canberra: AIHW. https://www.aihw.gov.au/reports/chronic-respiratory-conditions/asthma

Australian Institute of Health and Welfare 2019. *Chronic obstructive pulmonary disease (COPD)*. Cat. no. ACM 35. Canberra: AIHW. https://www.aihw.gov.au/reports/chronic-respiratory-conditions/copd

Balashazy, I. & Hoffman, W. 1995.Deposition of aerosols in asymmetric airway bifurcations. *Journal of Aerosol Science* 26, no. 2: 273-292.

Borgstrom, L., Olsson, B. &Thorsson, L. 2006. Degree of Throat Deposition Can Explain the Variability in Lung Deposition of Inhaled Drugs. *Journal of Aerosol Medicine* 19, no. 4: 473-483.

Cebral, J.R. & Summers, S.M. 2004. Tracheal and central bronchial aerodynamics using virtual bronchoscopy and computational fluid dynamics. *IEEE Transactions on Medical Imaging* 23, no. 8: 1021-1033.

Chan, T.L. & Lippmann, M. 1980. Experimental measurements and empirical modelling of the regional deposition of inhaled particles in humans. *The American Industrial Hygiene Association Journal* 41, no. 6: 399-409.

Cheng, KH. & Swift, D.L. 1995. Calculation of Total Deposition Fraction of Ultrafine Aerosols in Human Extrathoracic and Intrathoracic Regions. *Aerosol Science and Technology* 22, no. 2: 194-201.

D'Amato, G., Cecchi, L., D'Amato, M. &Liccardi, G. 2010. Urban air pollution and climate change as environmental risk factors of respiratory allergy: An update. *Journal of Investigational Allergology and Clinical Immunology* 20, no. 2: 95-102.

Davis, DL., Bell, ML. & Fletcher, T. 2002. A look back at the London smog of 1952 and the half century since. *Environmental Health Perspectives* 110, no. 12: A734-A735.

Dhand, R. 2008. Aerosol delivery during mechanical ventilation: from basic techniques to new devices. *J Aerosol Med Pulm Drug Deliv*. 21, no. 1: 45-60.

Dhand, R. 2017. How Should Aerosols Be Delivered During Invasive Mechanical Ventilation. *Respiratory Care*. 62, no. 10: 1343-1367.

Dominici, F., Peng, RD., Bell, ML., et al. 2006. Fine Particulate Air Pollution and Hospital Admission for Cardiovascular and Respiratory Diseases. *JAMA* 295, no. 10: 1127-1134.

Dugernier, J., Ehrmann, S., Sottiaux, T., et al. 2017. Aerosol delivery during invasive mechanical ventilation: a systematic review. *Crit Care* 21, no. 1.

Esther, P.H., Gordon, G.P. & Lawrence, D.L. 1973. Mathematical simulation of pulmonary O2 and CO2 exchange. *American Journal of Physiology* 224, no. 4: 904-917

Faria, A.C.D., Lopes, A.J., Jansen, J.M., et al. 2009. Influence of the ageing process on the resistive and reactive properties of the respiratory system. *Clinics* 64, no. 11: 1065-1073.

Gauderman, W.J., Avol, E., Gilliland, F., et al. 2004. The Effect of Air Pollution on Lung Development from 10 to 18 Years of Age. *The New England Journal of Medicine* 352: 1057-1067.

Gemci, T., Ponyavin, V., Chen, Y., Chen, H. & Collins, R. 2007. CFD Simulation of Airflow in a 17-Generation Digital Reference Model of the Human Bronchial Tree. *Journal of Applied Biomechanics* 23, no. 1.

Ghosh, A., Islam, M.S. & Saha, S.C. 2020. Targeted Drug Delivery of Magnetic Nano-Particle in the Specific Lung Region. *Computation* 8, no. 1: 10.

Gu, Q., Qi, S., Yue, Y., et al. 2019. Structural and functional alterations of the tracheobronchial tree after left upper pulmonary lobectomy for lung cancer. *Biomedical engineering online* 18, no. 1: 1-18.

Guan, WJ., Zheng, XY., Chung, KF., & Zhong, NS. 2016. Impact of air pollution on the burden of chronic respiratory diseases in China: time for urgent action. *The Lancent* 388, no. 10054: 15-21.

Hendryx, M., Islam, M.S., Dong, G.-H., et al. 2020. Air Pollution Emissions 2008-2018 from Australian Coal Mining: Implications for Public and Occupational Health. *International Journal of Environmental Research and Public Health* 17, no. 5: 1570.

Hess, D.R., Anderson, P., Dhand, R., et al. 2005. Device selection and outcomes of aerosol therapy: Evidence-based guidelines. *Chest* 127, no. 1:335-371.

Heyder, J., Gebhart, J., Rudolf, G., et al. 1986. Deposition of particles in the human respiratory tract in the size range 0.005-15 μm. *Journal of Aerosol Science* 17: 811-825.

Hu, G., Zhong, N. & Ran, P. 2014. Air pollution and COPD in China. *Journal of Thoracic Disease* 7, no. 1: 59-66.

Isaacs, K.K &Martonen, T.B. 2005. Particle Deposition in Children's Lungs: Theory and Experiment. *Journal of Aerosol Medicine* 18, no. 3: 337-353.

Islam, M.S., Saha, S.C., Sauret, E., et al. 2015. Numerical investigation of aerosol particle transport and deposition in realistic lung airway. *Proceeding of the 6th International*

Conference on Computational Methods 2: 1-9.
Islam, M.S., Saha, S.C., Sauret, E., et al. 2017a. Ultrafine particle transport and deposition in a large scale 17-generationlung model. *Journal of Biomechanics* 64:16-25.
Islam, M.S., Saha, S.C., Sauret, E., et al. 2017b. Pulmonary aerosol transport and deposition analysis in upper 17 generations of the human respiratory tract. *Journal of Aerosol Science* 108: 29-43.
Islam, M.S., Saha, S.C., Sauret, E., et al. 2017c. Numerical investigation of diesel exhaust particle and deposition in the CT-scan based lung airway. *AIP Conference Proceedings* 1851, no.1: 020092.
Islam, M.S., Saha, S.C., Gemci, T., et al. 2018a. Polydisperse microparticle transport and deposition to the terminal bronchioles in a heterogeneous vasculature tree. *Scientific reports* 8, no. 1: 1-9.
Islam, M.S., Saha, S.C. & Young, P.M. 2018b. Aerosol Particle Transport and Deposition in a CT-Based Lung Airway for Helium-Oxygen Mixture. *Proceedings of the 21st Australasian Fluid Mechanics Conference Adelaide Australia, Adelaide, Australia*: 10-13.
Islam, M.S., Saha, S.C., Gemci, T., et al. 2019a. Euler-Lagrange Prediction of Diesel-Exhaust Polydisperse Particle Transport and Deposition in Lung: Anatomy and Turbulence Effects. *Scientific Reports* 9, no. 1: 1-16.
Islam, M.S., Saha, S.C., Sauret, E., et al. 2019b. Euler-Lagrange approach to investigate respiratory anatomical shape effects on aerosol particle transport and deposition. *Toxicology Research and Application* 3.
Islam, M.S., Gu, Y.T., Farkas, A., et al. 2020a. Helium-Oxygen Mixture Model for Particle Transport in CT-Based Upper Airways. *International Journal of Environmental Research and Public Health* 17, no. 10: 3574.
Islam, M.S., Paul, G., Ong, H.X., et al. 2020b. A Review of Respiratory Anatomical Development, Air Flow Characterization and Particle Deposition. *International Journal of Environmental Research and Public Health* 17, no. 2: 380.
Kim, D., Chen, Z., Zhou, L.F. & Huang, SX. 2018. Air pollutants and early origins of respiratory diseases. *Chronic Diseases and Translational Medicine* 4, no. 2: 75-94.
Kim, JW., Heise, R.L., Reynolds, A.M., et al. 2017. Aging effects on airflow dynamics and lung function in human bronchioles. *PLoS One*12, no. 8.
Kleinstreuer, C. & Zhang, Z. 2003. Targeted drug aerosol deposition analysis for a four-generation pulmonary airway model with hemispherical tumors. *Journal of Biomechanical Engineering* 125, no. 2: 197-206.
Koullapis, P.G., Kassinos, S.C., Bivolarova, M.P., et al. 2016. Particle deposition in a realistic geometry of the human conducting airways: Effects of inlet velocity profile, inhalation flowrate and electrostatic charge. *Journal of Biomechanics* 49, no. 11: 2201-2212.
Kurt, OK., Zhang, J. & Pinkerton, KE. 2016. Pulmonary health effects of air pollution. *Current Opinion in Pulmonary Medicine* 22, no. 2: 138-143.
Lalas, A., Nousias, S., Kikidis, D., et al. 2017. Substance deposition assessment in obstructed pulmonary system through numerical characterization of airflow and inhaled particles attributes. *BMC Medical Informatics and Decision Making*. 17, no. 173.
Lai-Fook, S.J. & Hyatt, R.E. 2000. Effects of age on elastic moduli of human lungs. *Journal of applied physiology* 89, no. 1: 163-168.
Lee, D.Y. & Lee, J.W. 2002. Dispersion of aerosol bolus during one respiration cycle in a model of lung airways. *Journal of Aerosol Science* 33, no. 9: 1219-1234.
Lippmann, M. 1977. Regional deposition of particles in the human respiratory tract. *Comprehensive Physiology*.
Liu, Y., So, R.M.C. & Zhang, C.H. 2003. Modeling the bifurcating flow in an asymmetric

human lung airway. *Journal of Biomechanics* 36, no. 7: 951-959.
Ma, B. & Lutchen, K.R. 2009. CFD Simulation of Aerosol Deposition in an Anatomically Based Human Large-Medium Airway Model. *Annals of Biomedical Engineering*37, no. 271.
Mauderly, J.L. & Hahn, F.F 1982. The effects of age on lung function and structure of adult animals. *Adv. Vet. Sci. Comp. Med*. 26: 35-77.
Moss, O.R. & Oldham, M.J. 2006. Dosimetry Counts: Molecular Hypersensitivity May Not Drive Pulmonary Hyperresponsiveness.*Journal of Aerosol Medicine* 19, no. 4: 555-564.
Nowak, N., Kakade, P.P. & Annapragada, A.V. 2003. Computational Fluid Dynamics Simulation of Airflow and Aerosol Deposition in Human Lungs. *Annals of Biomedical Engineering* 31, no. 5: 374-390.
Phalen, R.F. & Oldham, M.J. 2001. Methods for modeling particle deposition as a function of age. *Respiration Physiology* 128, no.1: 119-130.
Polger, G. & Weng, T.R. 1979. The functional development of the respiratory system: from the period of gestation to adulthood. Am. Rev. Respir. Dis. 120: 625-695.
Rahman, M.M., Zhao, M., Islam, M.S, et al. 2019. Airflow dynamics and aerosol particle transport in a human lung. *Proceeding of the 1st International Conference on Mechanical and Manufacturing Engineering Research and Practice (iCMMERP-2019)*: 5-6.
Rahman, M.M., Zhao, M., Islam, M.S, et al. 2020. Airflow dynamic and particle deposition in age-specific human lungs. Brisbane, Australia: The University of Queensland.
Saber, E.M. &Heydari, G. 2012. Flow patterns and deposition fraction of particles in the range of 0.1-10 μm at trachea and the first third generations under different breathing conditions. *Computers in Biology and Medicine* 42, no. 5: 631-638.
Saha, S.C., Islam, M.S., Rahimi-Gorji, M., et al. 2019. Aerosol Particle Transport and Deposition in a CT-Scan Based Mouth-Throat Model. *AIP Conference Proceedings 2121*, no. 1: 040011.
Saha, S.C. & Islam, M.S. 2021. Airflow and Particle Transport to the Terminal Bronchioles During Heliox Breathing. In *Proceedings of 16th Asian Congress of Fluid Mechanics*, ed. L. Venkatakrishnan, S. Majumdar, G. Subramanian, et al., 535-544. Singapore, Springer.
Schiavoni, G., D'Amato, G. &Afferni, C. 2017. The dangerous liaison between pollens and pollution in respiratory allergy. *Annals of Allergy Asthma & Immunology* 118, no. 3: 269-275.
Sharma, G. & Goodwin, J. 2006. Effect of aging on respiratory system physiology and immunology. *Clinical Interventions in Aging* 1, no. 3: 253-260.
Shi, H., Kleinstreuer, C. & Zhang, Z. 2004. Nanoparticle transport and deposition in bifurcating tubes with different inlet conditions. *Physics of Fluids* 16, no. 7 2199-2213.
Singh, P., Raghav, V., Padhmashali, V., et al. 2020. Airflow and Particle Transport Prediction through Stenosis Airways. *International Journal of Environmental Research and Public Health* 17, no. 3.
Srivastav, V.K., Paul, A.R. and Jain, A., 2013. Effects of cartilaginous rings on airflow and particle transport through simplified and realistic models of human upper respiratory tracts, *Acta Mechanica Sinica* 29(6):883–892. DOI: 10.1007/s10409-013-0086-2
Srivastav, V.K., Kumar, A., Shukla, S.K., Paul, A.R., Bhatt, A.D. and Jain, A. 2014. Airflow and aerosol-drug delivery in a CT scan based human respiratory tract with tumor using CFD, *Journal of Applied Fluid Mechanics* 7(2): 345-356.
Srivastav, V.K., Paul, A.R. and Jain, A., 2019. Capturing the wall turbulence in CFD simulation of human respiratory tract, Mathematics and Computers in Simulation 160 (6): 23-38. DOI: 10.1016/j.matcom.2018.11.019
Sul, B., Wallqvist, A., Morris, MJ., et al. 2014. Computational study of the respiratory airflow characteristics in normal and obstructed human airways. *Computers in Biology and*

Medicine 52: 130-143.
Tsuda, A., Henry, F.S. & Butler, J.P. 2011. Particle Transport and Deposition: Basic Physics of Particle Kinetics. *Comprehensive Physiology* 3, no. 4: 1437-1471.
Tu, J., Yeoh, GH. & Liu, C. 2012. *Computational Fluid Dynamics: A Practical Approach*. 2nd edn. Elsevier. USA.
Van Ertbruggen, C., Hirsch, C. & Paiva, M. 2005. Anatomically based three-dimensional model of airways to simulate flow and particle transport using computational fluid dynamics. *J Appl Physiol (1985)* 98, no. 3: 970-980.
Verbeken, E.K., Cauberghs, M., Mertens, I., et al. 1992. The senile lung: comparison with normal and emphysematous lungs1. Structural Aspects. Chest 101, no. 3: 793-799.
Vestbo, J., Hurd, S.S., Agusti, A.G., et al. 2013. Global Strategy for the Diagnosis, Management, and Prevention of Chronic Obstructive Pulmonary Disease: GOLD Executive Summary. *American Journal of Respiratory and Critical Care Medicine* 187, no. 4: 347-365.
Vicente, E., Almengor, J.C., Caballero, L.A. & Campo, J.C. 2011. Invasive Mechanical Ventilation in COPD and Asthma. *Medicina Intensiva* 35, no. 5: 288-298.
Weibel, E.R. 1963. Morphometry of the Human Lung.*Sci Direct*.
World Health Organization 2020. Monitoring Health for the Sustainable Development Goals. *World Health Statistics*. https://www.who.int/gho/publications/world_health_statistics/en/
Xia, G., Tawhai, M.H., Hoffman, E.A., et al. 2010. Airway wall stiffening increases peak wall shear stress: a fluid-structure interaction study in rigid and compliant airways. *Annals of biomedical engineering* 38, no.5: 1836-1853.
Yao, H. & Rahman, I. 2011. Current concepts on oxidative/carbonyl stress, inflammation and epigenetics in pathogenesis of chronic obstructive pulmonary disease. *Toxicology and Applied Pharmacology* 254, no. 2: 72-85.
Yu, C. & Diu, C. 1982. A comparative study of aerosol deposition in different lung models. *The American Industrial Hygiene Association* Journal 43: 54-65.
Zhang, B., Qi, S., Yue, Y., et al. 2018. Particle Disposition in the Realistic Airway Tree Models of Subjects with Tracheal Bronchus and COPD. *BioMed Research International* 2018: 1-15.
Zhang, Z. & Kleinstresuer, C. 2001. Effect of Particle Inlet Distributions on Deposition in a Triple Bifurcation Lung Airway Model.*Journal of Aerosol Medicine* 14, no. 1: 13-29.
Zhang, Z. & Kleinstreure, C. 2004. Airflow structures and nano-particle deposition in a human upper airway model. *Journal of Computational Physics* 198, no. 1: 178-210.